Precambrian Research 187 (2011) 1–14

Contents lists available at ScienceDirect

Precambrian Research

journal homepage: www.elsevier.com/locate/precamres

Reworking of the Tarim Craton by underplating of mantle plume-derived magmas: Evidence from Neoproterozoic granitoids in the Kuluketage area, NW China

Xiaoping Long[a], Chao Yuan[a,*], Min Sun[b], Alfred Kröner[c], Guochun Zhao[b], Simon Wilde[d], Aiqin Hu[a]

[a] Key Laboratory of Isotope Geochronology and Geochemistry, Guangzhou Institute of Geochemistry, Chinese Academy of Sciences, Guangzhou 510640, China
[b] Department of Earth Sciences, The University of Hong Kong, Pokfulam Road, Hong Kong, China
[c] Institut für Geowissenschaften, Universität Mainz, D-55099 Mainz, Germany
[d] Department of Applied Geology, Curtin University of Technology, Perth, WA 6845, Australia

ARTICLE INFO

Article history:
Received 4 September 2010
Received in revised form 8 February 2011
Accepted 20 February 2011
Available online 21 March 2011

Keywords:
Craton reworking
Adakitic rocks
Underplating
Mantle plume
Tarim

ABSTRACT

Most Neoproterozoic granitoids in the Kuluketage area, northern Tarim Craton are characterized by strongly depleted HREE abundances and high Sr/Y and $(La/Yb)_N$ ratios, showing typical geochemical features of adakitic rocks. Zircon U–Pb dating of three adakitic plutons yielded Neoproterozoic ages (754 ± 4, 790 ± 3 and 798 ± 3 Ma). The adakitic granitoids exhibit low MgO and TiO_2 contents. Their low Cr, Co and Ni abundances, low $\varepsilon_{Hf}(t)$ values (−21 to −11) and high FeO^T/MgO ratios (mostly 2.2–2.9) preclude the possibility of being derived from partial melts of delaminated lower crust. The relatively low $\varepsilon_{Hf}(t)$ values and old Hf two-stage model ages ($T^2_{DM} = 2.42$–3.02 Ga) of the adakitic granitoids are similar to those of the basement rocks in the northern Tarim Craton, suggesting that the adakitic rocks were generated by partial melting of basement rocks in a thickened lower crust. Apart from the adakitic granitoids, Neoproterozoic normal I-type granitoids with low Sr/Y and $(La/Yb)_N$ ratios are also exposed in this area, and their geochemistry indicates a crustal origin at a shallower depth. Zircon U–Pb dating of the I-type granitoids also yielded a Neoproterozoic age of 785 ± 8 Ma. The petrogenesis of the Neoproterozoic adakitic granitoids suggests that Neoproterozoic crustal thickness in the northern Tarim Craton must have been over 50 km. In combination with the occurrence of coeval mantle-derived dykes and bimodal volcanic rocks, a partial melting scheme triggered by underplating of mantle plume-derived magmas is proposed to interpret the formation of the Neoproterozoic adakitic and I-type granitoids. This model provides an alternative interpretation for the Neoproterozoic craton reworking happened in the Rodinia supercontinent.

1. Introduction

The longevity of cratons is commonly ascribed to their thick lithospheric roots (>200 km), which are characterized by geochemically depleted, compositionally dehydrated subcontinental lithospheric mantle (SCLM) (Boyd et al., 1985; Sleep, 2005; King, 2005). The refractory SCLM is physically buoyant and mechanically rigid and makes cratons keep stable during the process of convergence and divergence (Pollack, 1986; Sleep, 2003; Carlson et al., 2005). However, recent studies have demonstrated that not all Precambrian cratons can remain stable after their formation and some of them have been reactivated and re-juvenilized (Griffin et al., 1998; Menzies and Xu, 1998; Carlson et al., 2004; Wells and Hoisch, 2008; Zheng and Wu, 2009), such as the well documented North China Craton (NCC) (Xu, 2001; Gao et al., 2002, 2009; Zhang et al., 2003; Xu et al., 2004, 2009; Wu et al., 2005; Zheng et al., 2006; Zhu and Zheng, 2009). Mantle plume, a most important geodynamic regime for crust–mantle interaction, was demonstrated to have played a key role in the formation of Archean cratons, especially for the Archean subcontinental lithospheric mantle (Boyd, 1989; Pearson et al., 1995; Zhao et al., 1998, 1999, 2001; Wyman et al., 2002; Griffin et al., 2003; Arndt et al., 2009). On the other hand, mantle plume may also affect the evolution of old cratons. For example, some well-preserved Archean cratons (e.g. the Pillbara and Kaapvaal cratons) had undergone multiple episodes of mantle plume activities after their formations (de Wit et al., 1992; Arndt et al., 2002). Therefore, whether old cratons could be reworked by subsequent mantle plumes is a key issue in understanding the evolution of continents.

In the Neoproterozoic, a super mantle plume was suggested to exist beneath the Rodinia supercontinent (Li et al., 1999, 2008). As one of the main cratons of the Central Asia (Lu et al., 2003;

* Corresponding author. Tel.: +86 20 85291780; fax: +86 20 85291780.
E-mail address: yuanchao@gig.ac.cn (C. Yuan).

0301-9268/$ – see front matter © 2011 Elsevier B.V. All rights reserved.
doi:10.1016/j.precamres.2011.02.001

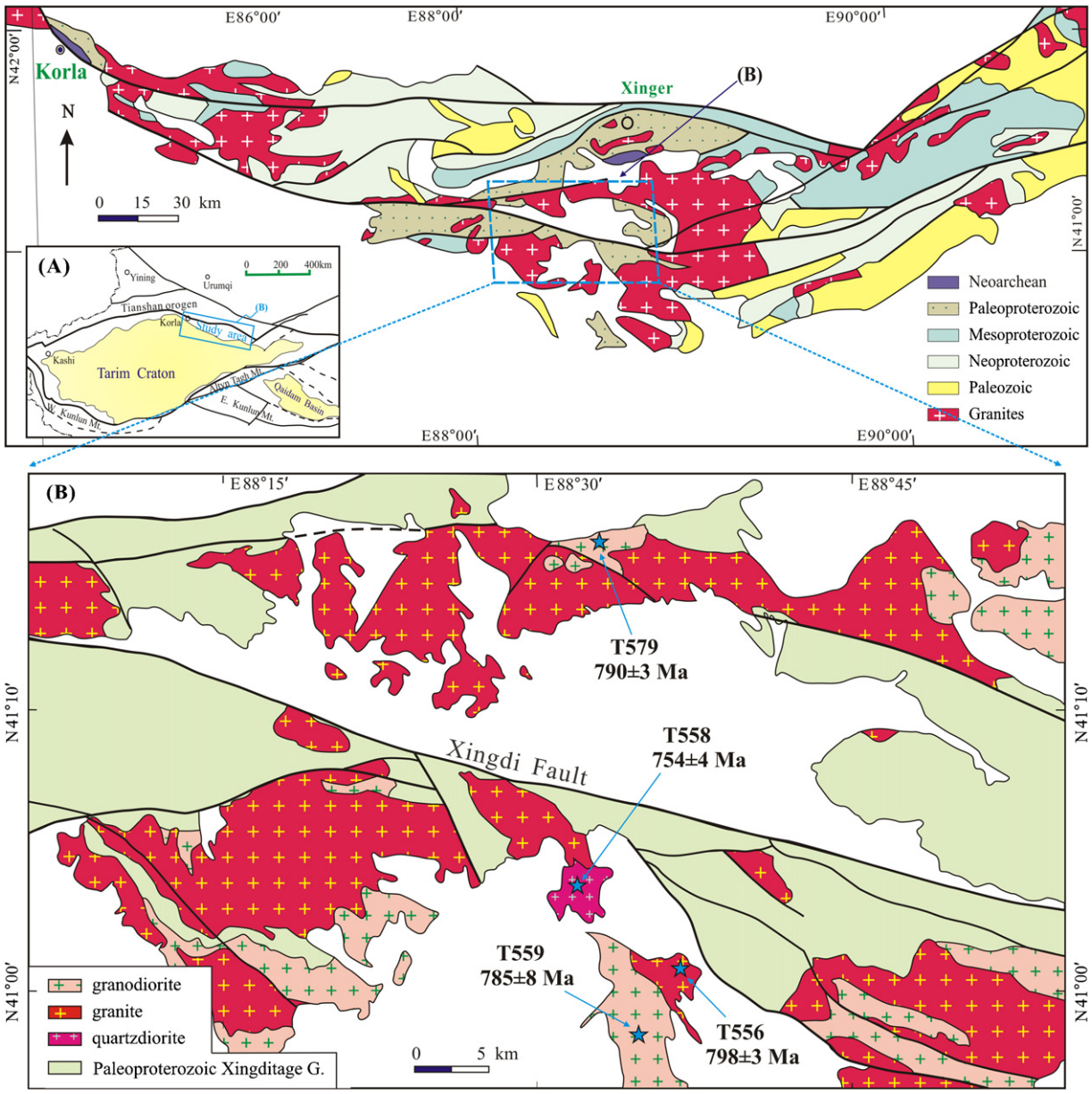

Fig. 1. Simplified geological map of the Kuluketage area, northern Tarim Craton. *Inset A*: an outline of the Tarim Craton and adjacent areas (modified from Lu et al., 2008); *Inset B*: geological map of the study area in the central Kuluketage area, northern Tarim Craton. Ages of samples analyzed in this study were marked in inset B.

Lu, 1992; Hu et al., 2000; Long et al., 2010; Shu et al., 2010), Tarim was considered as a part of the Rodinia supercontinent (Dalziel, 1991; Hoffman, 1991; Moores, 1991; Li et al., 2003b). Recent paleomagnetic data show similar calculated paleolatitudes from Neoproterozoic to early Paleozoic for Tarim, South China and Australia, indicating adjacent positions in the Rodinia supercontinent (Huang et al., 2005). Based on the Neoproterozoic rifting-related rock assemblages in these cratons, the super mantle plume was interpreted to lead to the breakup of Rodinia (Li et al., 2003b, 2008). Although the genesis of Neoproterozoic igneous rocks in South China remains controversial (Li et al., 2002, 2006; Zhou et al., 2006; Zhao and Zhou, 2007, 2008), the Precambrian Yangtze craton was suggested to have been reworked by the Neoproterozoic mantle plume (Li et al., 2003a,b; Zhang et al., 2009a). In the Tarim craton, intensive Neoproterozoic igneous rocks (e.g., adakitic rocks, mafic dykes, mafic complexes and bimodal volcanic rocks) were well preserved and recorded the interaction between cratonic lithosphere and mantle plume, which provide a good chance to understand the Neoproterozoic reworking of lithosphere not only in Tarim, but also in South China Block (SCB) and other old cratons in the supercontinent, and further give insights into the role of mantle plumes during craton reworking.

In this paper, we present new geochronological and geochemical data for Neoproterozoic adakitic and I-type granitoids in the Kuluketage area along the northern margin of the Tarim Craton (Fig. 1). These data provide new constraints on the age and petrogenesis of the Neoproterozoic igneous rocks, and thus we propose a new model of mantle plume-derived magma underplating not only to reconstruct Neoproterozoic geological evolution of the Tarim Craton, but also to interpret the formation of the ultramafic–mafic–carbonatite complex and mafic dykes in the Kuluketage area. This model also manifests that the underplating of plume-related mantle magmas would bring profound effects on the reworking of cratonic lithosphere.

2. Geological background and sample description

The Tarim Craton is dominantly covered by extensive Cenozoic sediments and its basement rocks mostly occur along the northern and eastern margins (Fig. 1, inset A). In the Kuluketage area, northern Tarim Craton, the oldest basement consists of tonalite–trondjemite–granodiorite (TTG) gneisses and supracrustal rocks which formed in the Neoarchean to early Paleoproterozoic (Hu et al., 2000; Hu and Wei, 2006; Guo et al., 2003; Lu et al., 2008; Shu et al., 2010; Long et al., 2011). The TTG gneisses consist of two types, characterized by high and low Sr/Y ratios, respectively (Long et al., 2010). The supracrustal rocks are dominated by sedimentary sequences with amphibolite layers, which were metamorphosed from an association of clastic sediments and intermediate to mafic volcanic rocks (Gao et al., 1993; Dong et al., 1998).

Precambrian sequences of metasediments are well exposed in the Kuluketage area and generally unconformably overlie the basement (Gao et al., 1993; BGMRX, 1993; Fig. 1). The Paleoproterozoic Xingditage Group and the Mesoproterozoic Aierjigan Group are typical marine sedimentary sequences consisting of clastic and carbonate rocks, covered by Neoproterozoic marine sediments (Gao et al., 1993; Hu et al., 1997; Lu et al., 2008). The Neoproterozoic strata are characterized by several layers of glacial deposits and volcanic rocks, separated by thick shale, sandstone and limestone units (Xu et al., 2005).

Neoproterozoic granitoids intrude the basement rocks and Paleoproterozoic to Mesoproterozoic sedimentary sequences and are dominated by slightly gneissic biotite granite and granodiorite (Fig. 1). Some of these granitoids are adakitic in composition, and recent zircon dating yielded two Neoproterozoic ages of 795 ± 10 and 820 ± 10 Ma, which are synchronous with an ultramafic–mafic–carbonatite complex in the area (810 ± 6 Ma) (Zhang et al., 2007). On the south side of the Xingdi fault, biotite granite was intruded by a small quartzdiorite pluton (Fig. 1, inset B). In this area, northwest-trending mafic dyke swarms intruded into the Neoproterozoic granitoids except for the small quartzdiorite pluton.

Samples of Neoproterozoic granite, granodiorite and quartzdiorite in the central Kuluketage area were collected for geochronological and geochemical studies (Fig. 1, inset B). The biotite granite is the most widespread igneous rock in the study area. It is slightly gneissic and exhibits an inequigranular texture with coarse (>0.5 cm) K-feldspar (45–55 vol.%) and medium to coarse (0.2–0.4 cm) quartz (20–25 vol.%), plagioclase (20–30 vol.%), and biotite (5–10 vol.%). The granodiorite is gray in color and consists of biotite and hornblende-biotite varieties. The rocks are predominantly composed of medium- to fine-grained (0.05–0.4 cm) quartz (10–20 vol.%), plagioclase (40–55 vol.%) and biotite (15–20 vol.%) with minor K-feldspar (<10 vol.%), hornblende (<10 vol.%) and accessory minerals, e.g. magnetite, titanite, apatite and zircon. The quartzdiorite sporadically occurs in the southern part of the study area, resembling the granodiorite but with less quartz (5–10 vol.%), more plagioclase (50–60 vol.%), and without K-feldspar and hornblende.

3. Analytical methods

3.1. Whole-rock geochemistry

Samples were crushed into small chips and ultrasonically cleaned in distilled water and dried, then powdered. Major element oxides (wt.%) were determined on fused glasses with a 1:8 sample to $Li_2B_4O_7$ flux ratio, using a Rigaku ZSX100e X-ray fluorescence spectrometer in the Key Laboratory of Isotope Geochronology and Geochemistry, Guangzhou Institute of Geochemistry. The accuracy of the XRF analyses is estimated at ca. 1% for SiO_2, ca. 5% for MnO and P_2O_5 and ca. 2% for other major oxides (Li et al., 2003a; Li, 1997). Trace elements, including rare earth elements (REE), were analyzed on a Perkin-Elmer Sciex ELAN 6000 ICP–MS in the Guangzhou Institute of Geochemistry, following procedures described by Li et al. (2002) and Li (1997). Powdered samples (50 mg) were digested with mixed HNO_3 + HF acid in steel-bomb coated Teflon beakers for two days in order to assure complete dissolution of the refractory minerals. An internal standard solution containing the single element Rh was used to monitor signal drift. USGS rock standards G-2, W-2, MRG-1 and AGV-1 and the Chinese national rock standards GSD-12, GSR-1, GSR-2 and GSR-3 were used to calibrate elemental concentrations of the measured samples. Analytical precision was generally better than 5%. The geochemical data are presented in Supplementary Table 1.

3.2. Zircon U–Pb dating and Hf isotope analyses

Zircons were separated by heavy liquid and magnetic techniques and purified by handpicking under a binocular microscope. Zircon grains were then picked and mounted on adhesive tape and enclosed in epoxy resin and polished to about half their diameter. In order to observe the internal textures of the polished zircons, cathodoluminescence (CL) imaging was carried out using a JXA-8100 Electron Probe Microanalyzer with a Mono CL3 Cathodoluminescence System for high resolution imaging and spectroscopy in the Guangzhou Institute of Geochemistry, Chinese Academy of Sciences. CL images of typical zircons are presented in Fig. 2.

3.2.1. U–Pb dating

Zircon U–Pb dating was performed by LA-ICPMS in the Institute of Geology and Geophysics, the Chinese Academy of Sciences, Beijing. A Geolas-193 laser-ablation system equipped with a 193 nm ArF-excimer laser was used in connection with an ELAN6100 DRC ICP–MS. Helium was used as the carrier gas to enhance the transport efficiency of the ablated material. The helium carrier gas inside the ablation cell was mixed with argon gas before entering the ICP to maintain stable and optimum excitation conditions. The analyses were conducted with a beam diameter of 63 μm with a typical ablation time of about 30 s for 200 cycles of each measurement, a 10 Hz repetition rate, and a laser power of 100 mJ/pulse (Wu et al., 2006). Zircon 91500 was used as the standard, and the silicate glass NIST 610 was used to optimize the instrument. The following masses were measured: ^{202}Hg, ^{204}(Pb + Hg), ^{206}Pb, ^{207}Pb, ^{208}Pb, ^{232}Th, ^{235}U, and ^{238}U. Raw count rates for ^{29}Si, ^{204}Pb, ^{206}Pb, ^{207}Pb, ^{208}Pb, ^{232}Th and ^{238}U were collected for age determination. ^{202}Hg is usually <10 cps in the gas blank, therefore the contribution of ^{204}Hg to ^{204}Pb is negligible and is not considered further. The integration time for the four Pb isotopes was 63 ms, whereas for the other isotopes (including ^{29}Si, ^{232}Th and ^{238}U) it was 30 ms (Xie et al., 2008). The average gas blank was typically <4000 cps for ^{29}Si; <10 cps for ^{204}Pb, ^{206}Pb, ^{207}Pb and ^{208}Pb; <1 cps for ^{232}Th and ^{238}U. Uranium, Th and Pb concentrations were calibrated by using ^{29}Si as the internal standard and NIST SRM 610 as the external standard. ^{207}Pb/^{206}Pb and ^{206}Pb/^{238}U ratios were calculated using the GLITTER 4.0 program (Jackson et al., 2004) and then corrected using the Harvard zircon 91500 as external standard. The detailed analytical technique was described by Xie et al. (2008). The common-Pb correction followed the method described by Andersen (2002). U, Th and Pb concentrations were calibrated using ^{29}Si as an internal standard and NIST 610 as reference material. The age calculation and plotting of concordia diagrams was performed using Isoplot/Ex 3.0 (Ludwig, 2003). A mean ^{206}Pb/^{238}U age (1064.5 ± 7.2 Ma, 2σ) is obtained for 35 spots of the standard 91500, which is in good agreement with the recommended ^{206}Pb/^{238}U age (1065.4 ± 0.6 Ma,

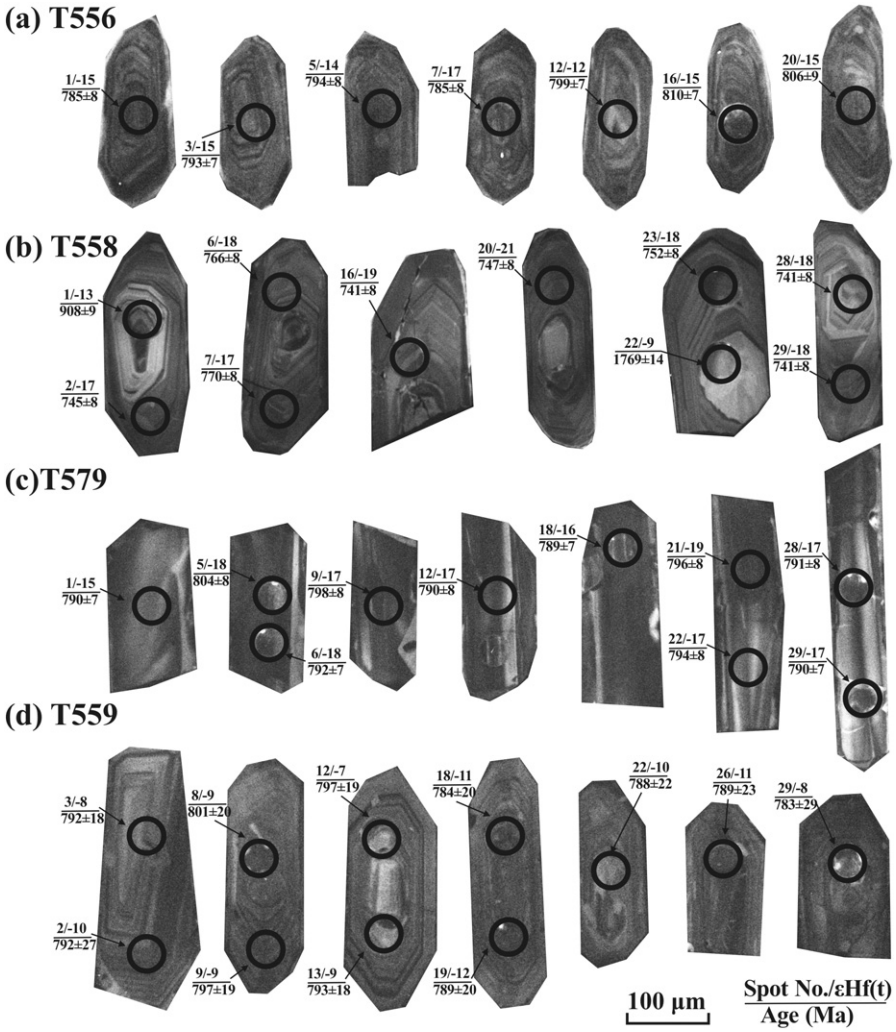

Fig. 2. Representative cathodoluminescence images for zircon samples. $^{206}Pb/^{238}U$ ages for dominate zircons (<1000 Ma) are marked with black circles while $^{207}Pb/^{206}Pb$ ages for inherited cores (>1000 Ma) are marked with white circles.

2σ; Wiedenbeck et al., 1995). The age data are presented in Supplementary Table 2.

3.2.2. Lu–Hf isotope analysis

Zircon Lu–Hf isotope analysis was carried out by means of LA–MC–ICPMS in the same lab as the U–Pb dating. Before entering the ICPMS for U–Pb isotopic analysis, the mixed carrier gas was separated into two parts. One part transported the ablated sample material to the Neptune multi-collector ICPMS torch. This instrument has a double focusing multi-collector ICP–MS and has the capability of high mass resolution measurements in multiple collector mode. It is equipped with eight motorized Faraday cups and five fixed central ion channels. During Hf analyses, isobaric interference corrections of ^{176}Lu and ^{176}Yb on ^{176}Hf have been precisely processed. Due to the extremely low $^{176}Lu/^{177}Hf$ in zircon (normally <0.002), the isobaric interference of ^{176}Lu on ^{176}Hf is negligible (Iizuka and Hirata, 2005). Based on evaluation of five methods of correction to the isotopic interference of ^{176}Yb on ^{176}Hf in the previous literature, the mean β_{Yb} value in the same spot was recommended (Wu et al., 2006). The interference of ^{176}Yb on ^{176}Hf was corrected by measuring the interference-free ^{172}Yb isotope and using a recommended $^{176}Yb/^{172}Yb$ ratio of 0.5886 (Chu et al., 2002) to calculate $^{176}Hf/^{177}Hf$ ratios. In doing so, a mean $^{173}Yb/^{171}Yb$ ratio for the analyzed spot itself was automatically used in the same run to calculate a mean β_{Yb} value, and then the ^{176}Yb signal intensity was calculated from the ^{173}Yb signal intensity and the mean β_{Yb} value (Iizuka and Hirata, 2005). The standard zircon 91500 was used in this correction for ^{176}Yb–^{176}Hf interference, showing variable $^{176}Yb/^{177}Hf$ ratios of 0.0066–0.0126 with an average of 0.0077 for standard 91500 (Wu et al., 2006). Detailed isobaric interference and analytical procedures are described by Wu et al. (2006) and Xie et al. (2008). The measured $^{176}Lu/^{177}Hf$ ratios and the ^{176}Lu decay constant of 1.867×10^{-11} yr^{-1} reported by Soderlund et al. (2004) were used to calculate initial $^{176}Hf/^{177}Hf$ ratios. Chondritic values of $^{176}Hf/^{177}Hf = 0.0336$ and $^{176}Lu/^{177}Hf = 0.282785$ reported by Bouvier et al. (2008) were used for the calculation of $\varepsilon_{Hf}(t)$ values. The depleted mantle line is defined by present-day $^{176}Hf/^{177}Hf = 0.28325$ and $^{176}Lu/^{177}Hf = 0.0384$ (Griffin et al., 2004). Because zircons are generally formed in granitic magma derived from felsic crust, two-stage model ages (T^2_{DM}) are more meaningful than the depleted mantle model ages. The mean $^{176}Lu/^{177}Hf$ ratio of 0.015 for the average continental crust (Griffin et al., 2002) was used to calculate T^2_{DM}. During the analysis process, a mean $^{176}Hf/^{177}Hf$ ratio of 0.282309 ± 11 (2σ) was obtained for the standard zircon 91500 which is identical to a recommended value of 0.282306 ± 8 (2σ) by the solution method (Woodhead et al., 2004). The Hf isotopic data are listed in Supplementary Table 3.

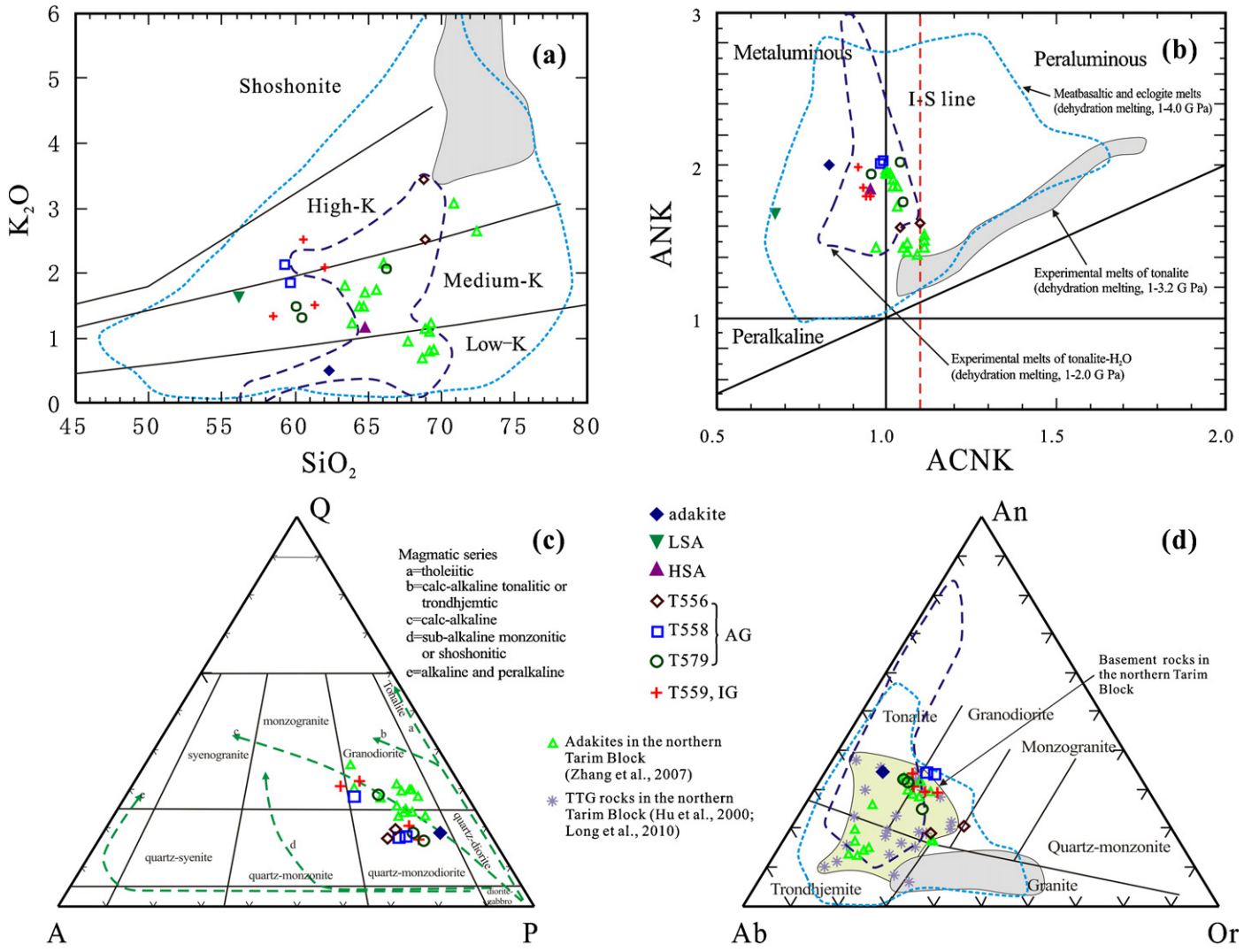

Fig. 3. Geochemical classification diagrams for Neoproterozoic granitoids in the Kuluketage area. (a) SiO_2–K_2O diagram (after Le Maitre, 1989); (b) ACNK versus ANK diagram (after Maniar and Piccoli, 1989); (c) QAP diagram (Streckeisen, 1976) with chemical trends (dashed arrows) of Lameyre and Bowden (1982) for granitoids of Tromai Intrusive Suite and Negra Velha Granite; (d) Normative feldspar classification of O'Connor (1965). Adakite data from Condie (2005) and data for low-SiO_2 and high-SiO_2 adakite from Martin et al. (2005). Field of metabasaltic and eclogitic melts (dehydration melting) (1–4.0 GPa), tonalite–H_2O melts (1–2.0 GPa), and tonalite dehydration melts (1–3.2 GPa) are from Wang et al. (2007a) and references therein.

4. Results

4.1. Geochemistry

Samples of the Neoproterozoic granitoids from the northern Tarim Craton display distinct geochemical characteristics. Based on Sr/Y ratios, these rocks can be divided into two groups, including adakitic granitoid (AG) (Sr/Y > 60) and normal I-type granitoid (IG) (Sr/Y < 36) (Supplementary Table 1).

4.1.1. Adakitic granitoid (AG)

Most granitoids in this area are dominated by such kind of rocks, which exhibit a wide variation of SiO_2 contents (59.39–68.94 wt.%) and medium to high K_2O contents (2.09–3.86 wt.%) (Fig. 3a). The AG samples are composed of different rock types, including quartzdiorite, biotite granite and granodiorite. The quartzdiorite possesses the lowest SiO_2 contents (59.39–59.78 wt.%) while the biotite granite has the highest SiO_2 contents (68.86–68.94 wt.%). The quartzdiorite has higher Al_2O_3, $Fe_2O_3^T$, MgO, CaO, TiO_2 and P_2O_5 than the biotite granite (Fig. 4a–d). The AG samples display a large variation in Na_2O/K_2O ratios (0.83–1.97) and $Mg^{\#}$ values (38–56). All samples of the AG possess low ASI indexes (A/CNK = $[Al_2O_3/(CaO + Na_2O + K_2O)$ mol%]) varying from 0.98 to 1.10, indicating metaluminous to slightly peraluminous composition (Fig. 3b). In the normative Q–A–P diagram (Fig. 3c), these samples mostly fall in granodiorite and quartz-monzodiorite fields. In the normative feldspar classification diagram (Fig. 3d), the AG samples mainly plot in granodiorite field.

The AG samples have low Cr (12.0–25.1 ppm), Co (<13 ppm) and Ni (<9 ppm) contents (Fig. 4e–f). Samples from this group are characterized by high Sr (630–1000 ppm) and low Y (4.78–16.8 ppm) contents with high Sr/Y ratios (60–133), higher than those of the average high-SiO_2 adakite (Sr/Y = 57, Martin et al., 2005). In the chondrite-normalized REE patterns and primitive mantle-normalized trace element diagrams (Fig. 5a–b), the AG samples are all enriched in light REEs ($(La/Yb)_N$ = 36–60) and show pronounced negative Nb–Ta anomalies. Among these rocks, the quartzdiorite samples have relative high heavy REE contents and show slightly negative Eu anomalies with Eu/Eu^* between 0.86 and 0.92. Apart from the quartzdiorite, other AG samples mostly exhibit positive Eu anomalies with Eu/Eu^* values ranging from 1.01 to 1.24, resembling the average adakite (Martin et al., 2005).

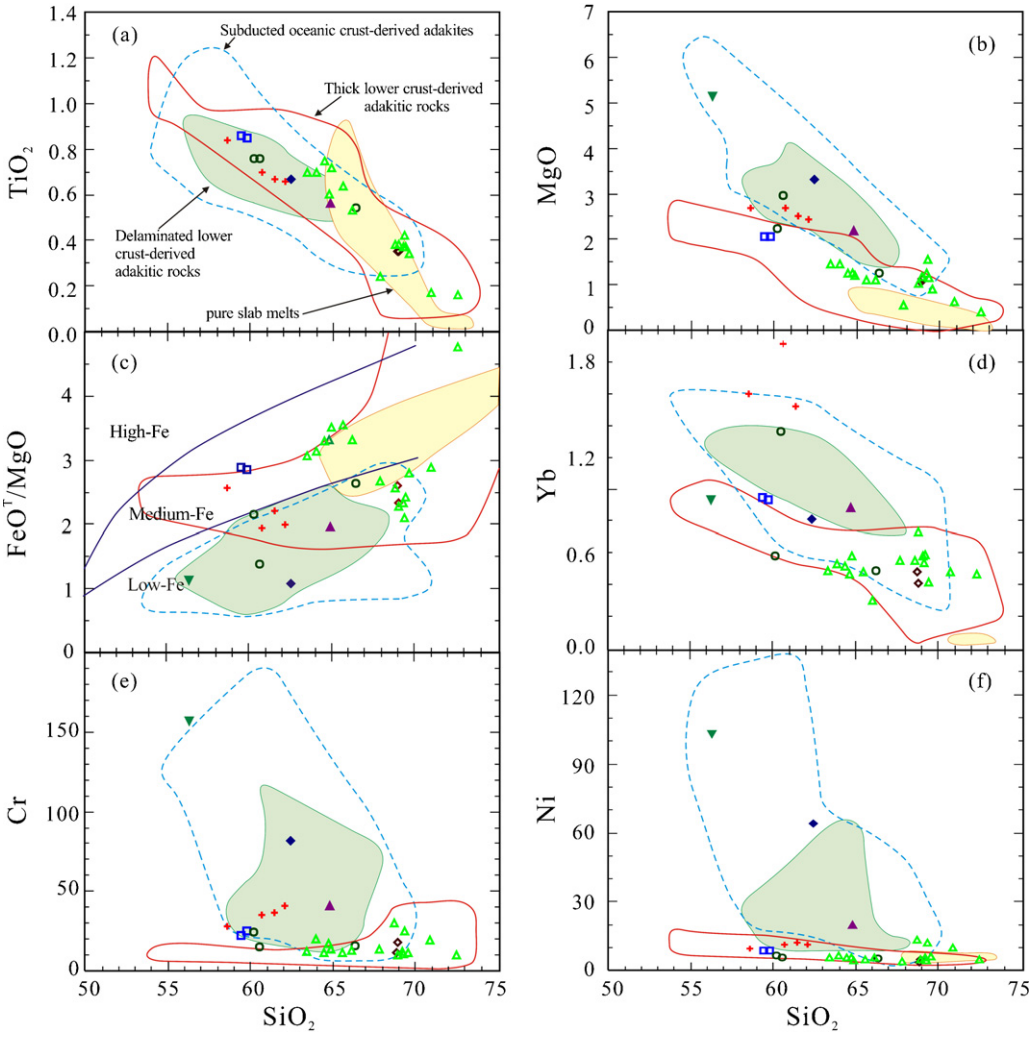

Fig. 4. Harker diagrams for the Neoproterozoic granitoids. Reference fields are from Wang et al. (2006) and references therein. Symbols are identical to those in Fig. 3.

4.1.2. Normal I-type granitoid (IG)

Samples of this group are hornblende-biotite granitoid. They show a relatively narrow range of SiO_2 contents (58.56–62.06 wt.%) (Fig. 3a). The IG samples have higher $Fe_2O_3^T$ (5.39–7.61 wt.%), MgO (2.44–2.68 wt.%), CaO (4.49–5.43 wt.%), TiO_2 (0.66–0.84 wt.%) and lower K_2O (2.12–3.09 wt.%) contents, with higher Na_2O/K_2O (1.18–1.78) ratios than those of the biotite granite of the AG, but indistinguishable from other rocks of this group. The ASI index of the IG varies from 0.92 to 0.95, displaying a weakly metaluminous to slightly peraluminous composition (Fig. 3b). The IG samples plot in granodiorite and quartz-mozondiorite fields along the calc-alkaline trend in the normative Q–A–P diagram (Fig. 3c). In the normative feldspar classification diagram (Fig. 3d), the IG samples fall in the same field to the AG samples.

The IG samples exhibit Cr (27.8–41.1 ppm), Co (11.3–31.0 ppm) and Ni (9.55–12.0 ppm) contents slightly higher than those of the AG, but obviously lower than those of the average adakite (Martin et al., 2005). In comparison with the AG samples, the IG samples have lower Sr (592–697 ppm) and higher Y (17.6–23.8 ppm) contents and lower Sr/Y ratios (25–36). In the chondrite-normalized REE patterns (Fig. 5c), the IG samples are generally enriched in LREEs ($(La/Yb)_N$ = 14–19), with higher HREEs contents than the AG and the average adakite. The samples show moderate negative Eu anomalies with Eu/Eu^* between 0.62 and 0.84. In the primitive mantle-normalized trace element diagram (Fig. 5d), the samples are characterized by strong negative Nb–Ta anomalies with small Sr and Ti troughs.

4.2. U–Pb geochronology and Hf isotopic composition

4.2.1. Biotite granite (sample T556, AG)

Thirty-two zircons from the biotite granite (T556) were analyzed for U–Pb and Hf isotopic composition. The zircons are enhedral to subhedral, prismatic with length-to-width ratios ranging from 1.5 to 2.5. They are between 120 and 200 μm in size and have sharp prismatic terminations and concentric oscillatory zoning revealed by cathodoluminescence imaging (Fig. 2a), which, together with their high Th/U ratios (0.25–0.72), indicate an igneous origin. Thirty-one spots formed a $^{206}Pb/^{238}U$ age population ranging from 784 to 811 Ma, which yielded a weighted mean age of 798 ± 3 Ma (MSWD = 1.09, Fig. 6a). This age is therefore interpreted to reflect the time of crystallization of the granite. The zircons have higher initial Hf compositions ($^{176}Hf/^{177}Hf(t)$ = 0.281793–0.281954) than those from Paleoproterozoic to Archean TTG gneisses in the northern Tarim Craton (Fig. 7a, Long et al., 2010). The initial Hf compositions, together with their low $\varepsilon_{Hf}(t)$ values (−17 to −11, Fig. 7b), reveal an old crustal origin. In addition, an inherited core was found and yielded a $^{206}Pb/^{238}U$ age of 922 Ma, with Hf composition ($\varepsilon_{Hf}(t) = -11$) similar to those of the younger igneous grains.

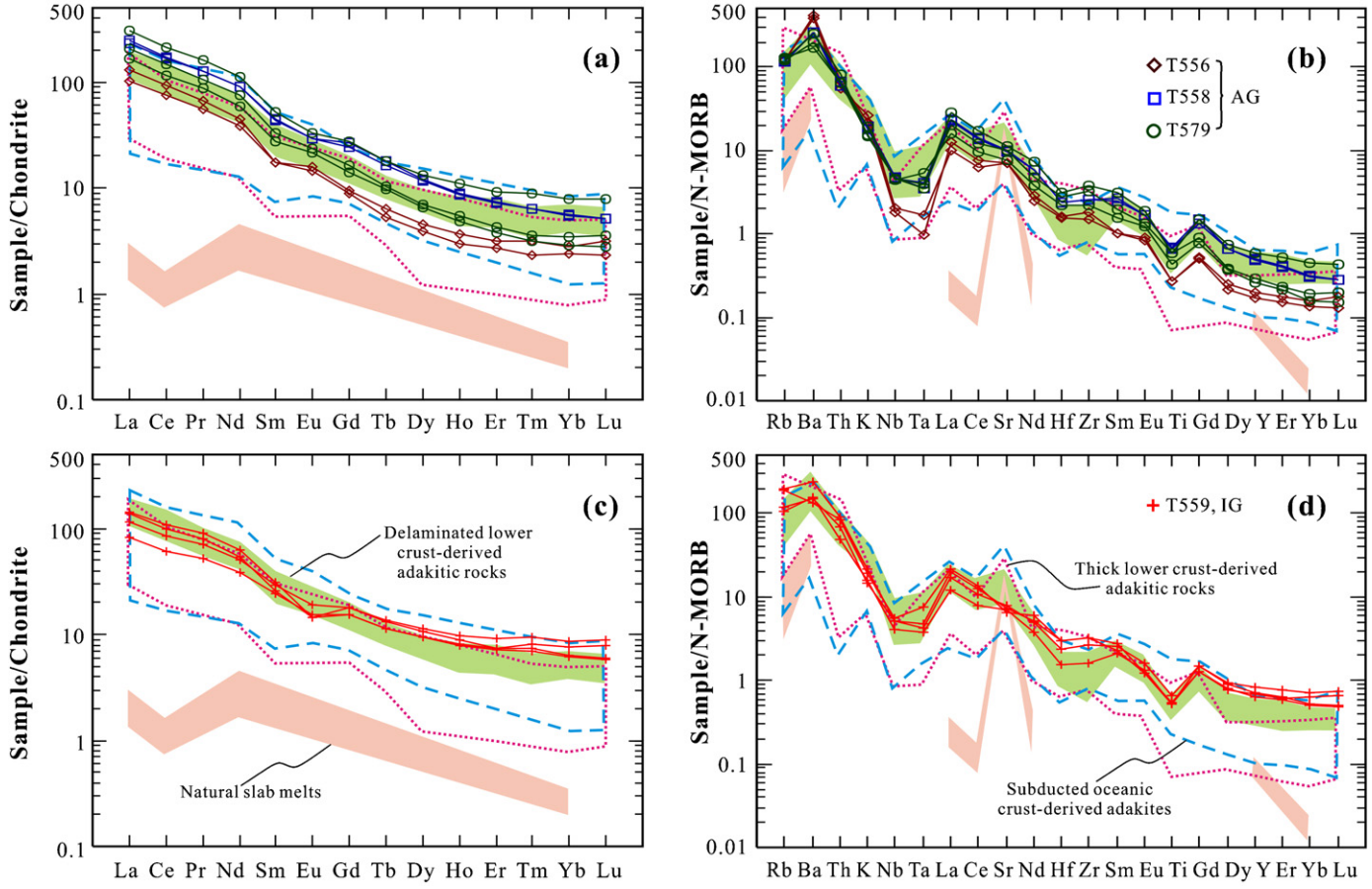

Fig. 5. Chondrite-normalized REE patterns and primitive mantle-normalized spider diagrams for the Neoproterozoic granitoids. Chondrite and N-MORB normalizing values from Sun and McDonough (1989), respectively. Reference fields are from Wang et al. (2006) and references therein.

4.2.2. Quartzdiorite (T558, AG)

Twenty-nine spots were analyzed on zircons from the quartzdiorite (T558). These grains are much bigger (120–250 μm) than zircons from the biotite granite and have elongation ratios ranging from 1.5 to 3. They are also euhedral to subhedral, prismatic and display clear oscillatory zoning (Fig. 2b). The spots exhibit high Th/U ratios (mostly >0.2; Supplementary Table 2), consistent with their igneous origin. Twenty-five analyses yielded $^{206}Pb/^{238}U$ ages between 741 and 771 Ma, which formed a weighted mean age of 754 ± 4 Ma (MSWD = 1.5, Fig. 6b). The mean age is therefore interpreted as the crystallization age of the quartzdiorite. The initial Hf compositions ($^{176}Hf/^{177}Hf(t)$ = 0.281713–0.281921) and $\varepsilon_{Hf}(t)$ values (−21 to −13) of these zircons are slightly lower than those of zircons from the biotite granite (Fig. 7).

A few zircons of the sample have inherited cores, which have high luminescence without clear oscillatory zoning (Fig. 2b). Among the four inherited cores, one yielded a Neoproterzoic $^{206}Pb/^{238}U$ age of 908 ± 9 Ma and three gave Paleoproterozoic $^{207}Pb/^{206}Pb$ ages around 1.77 Ga. The three Paleoproterozoic ages maybe reflect the metamorphic event of their source materials recorded by the metamorphic rims of zircons from the basement rocks (Long et al., 2010). These cores have lower initial Hf compositions ($^{176}Hf/^{177}Hf(t)$ = 0.281409–0.281848) and higher $\varepsilon_{Hf}(t)$ value (−3 to −13) than the younger zircons in this sample (Fig. 7).

4.2.3. Biotite granodiorite (T579, AG)

Most zircons from sample T579 are needle-shaped with elongation ratios greater than 2.0 (Fig. 2c). They have low luminescence and high Th/U ratios (mostly >0.8). Thirty-one zircon spots comprised a single $^{206}Pb/^{238}U$ age population ranging from 773 to 811 Ma and yielded a weighted mean age of 790 ± 3 Ma (MSWD = 0.81, Fig. 6c). This age is interpreted as the crystallization age of the rock. The zircons have high initial Hf compositions ($^{176}Hf/^{177}Hf(t)$ = 0.281741–0.281864) and low $\varepsilon_{Hf}(t)$ values between −19 and −15, resembling zircons from the coeval biotite granite.

4.2.4. Hornblende-biotite granodiorite (T559, IG)

Zircons from sample T559 are between 100 and 300 μm in size and generally euhedral, prismatic, with elongation ratios ranging from 1.2 to 3. They display clear concentric oscillatory zoning (Fig. 2d) and have high Th/U ratios (>0.2). Twenty-nine spots give $^{206}Pb/^{238}U$ ages between 730 and 802 Ma and yielded a weighted mean age of 785 ± 8 Ma (MSWD = 0.63, Fig. 6d), which is interpreted as the crystallization age of the I-type granitoid. Zircons from this sample exhibit the highest initial Hf compositions ($^{176}Hf/^{177}Hf(t)$ = 0.281940–0.282086) and their $\varepsilon_{Hf}(t)$ values (−12 to −7) are slightly higher than those of zircons from the other Neoproterozoic samples.

5. Petrogenesis

5.1. Petrogenesis of the AG

High Sr, low HREE and high Sr/Y and $(La/Yb)_N$ ratios of the Neoproterozoic AG rocks show typical characteristics of adakites (Fig. 8a–b). Five common petrogenesis models have been proposed to interpret the origin of the AG rocks, including: (1) partial melting of subducted basaltic slab (Defant and Drummond, 1990; Stern and Kilian, 1996; Martin et al., 2005); (2) partial melting of

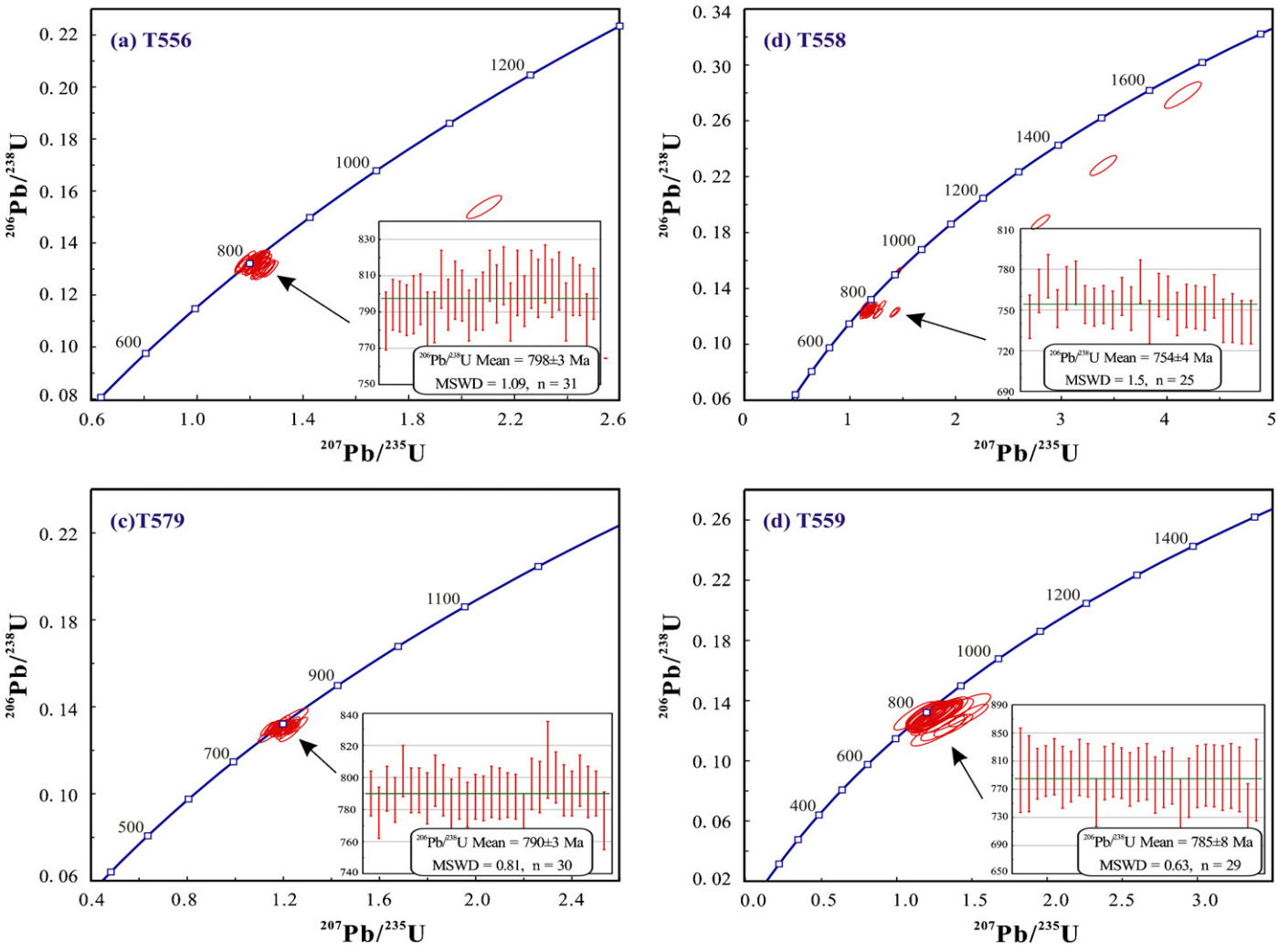

Fig. 6. U–Pb concordia diagrams for dated zircon samples.

slab-melt-modified peridotitic mantle wedge (Moyen et al., 2001; Martin et al., 2005); (3) crustal assimilation and fractional crystallization (AFC) processes of parental basaltic magmas (Castillo, 2006; Rodriguez et al., 2007; Guo et al., 2009); (4) partial melting of delaminated lower crust (Kay and Kay, 1993; Xu et al., 2002; Wang et al., 2007a); (5) partial melting of thickened lower crust (Muir et al., 1995; Petford and Atherton, 1996; Chung et al., 2003; Wang et al., 2005).

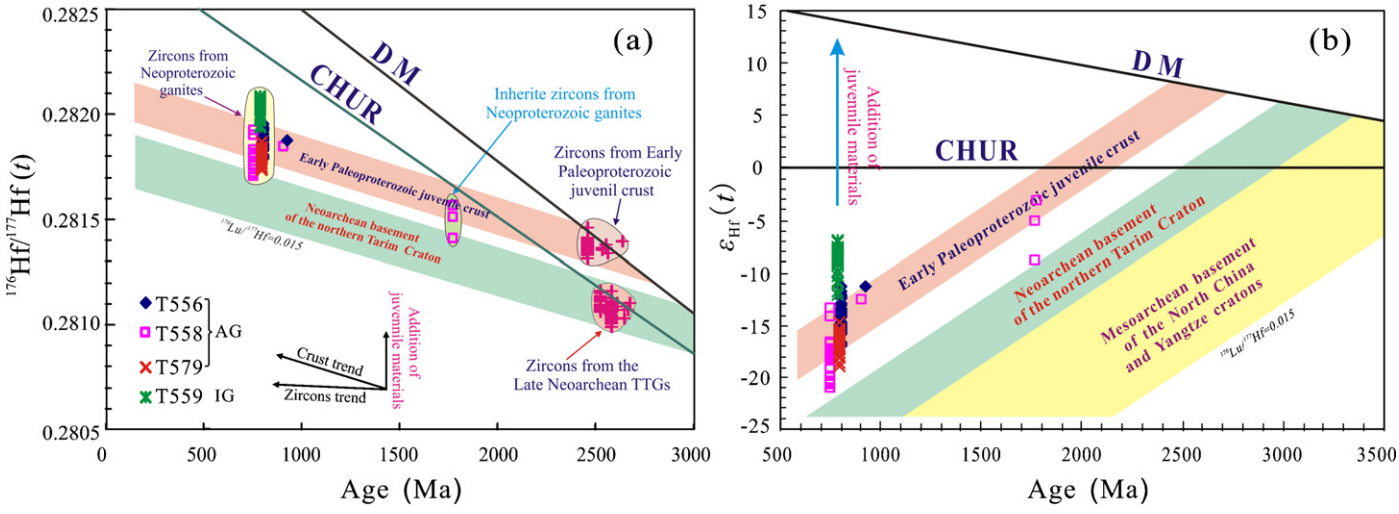

Fig. 7. Initial Hf composition and ε_{Hf} (t) versus crystal age plots for dated zircon samples. Fields for northern Tarim basement, North China and Yangtze cratons are based on data from Long et al. (2010) and references therein.

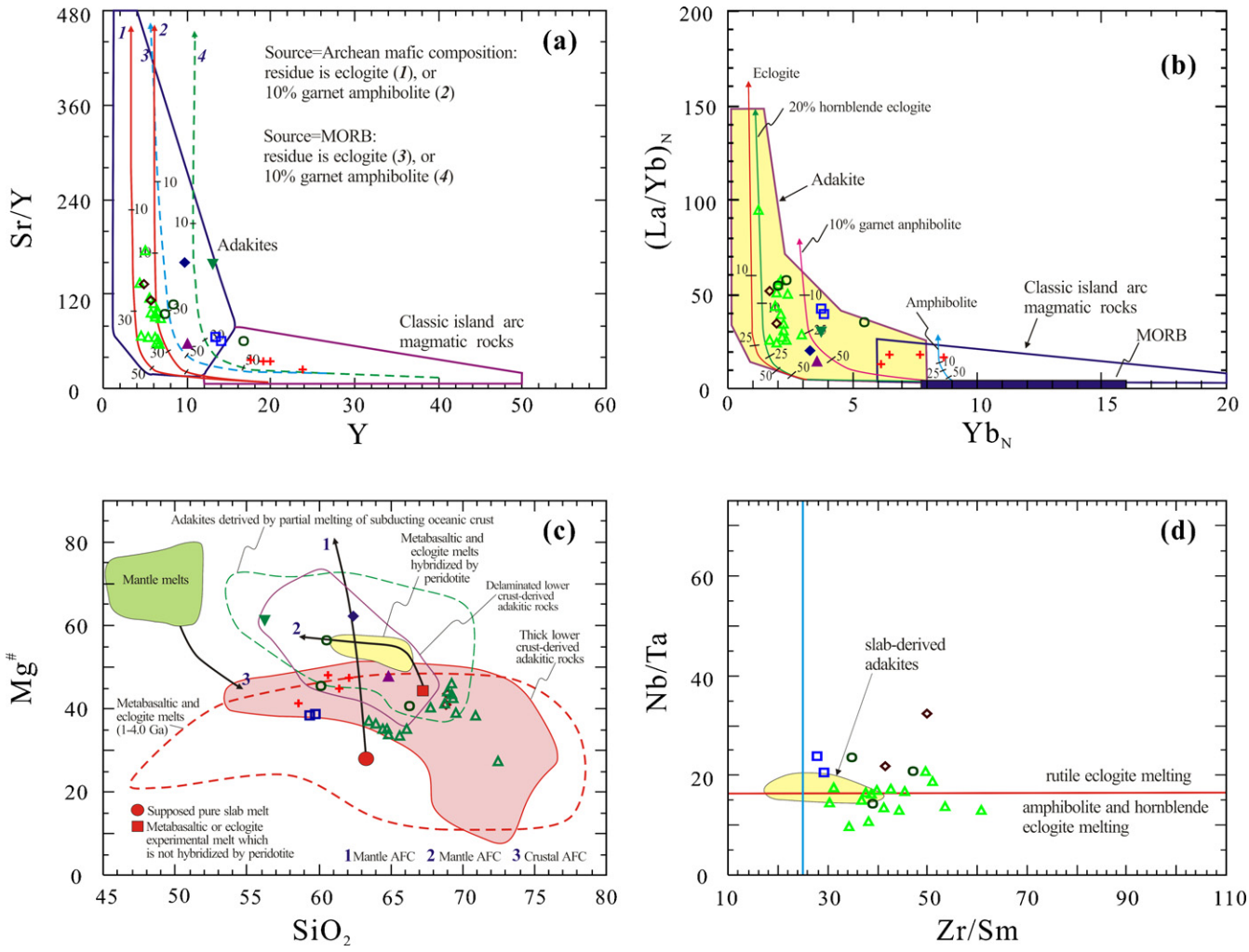

Fig. 8. (a–b) Plots of Sr/Y versus Y and $(La/Yb)_N$ versus Yb_N for the Neoproterozoic granitoids. Fields for adakites and classical island arc magmatic rocks are from Defant and Drummond (1990) and Martin et al. (2005). Partial melting curves for basalt leaving residues of eclogite, garnet amphibolite and amphibolite are from Defant and Drummond (1990); (c–d) SiO_2–$Mg^{\#}$ and Nb/Ta versus Zr/Sm diagram (after Martin et al., 2005). Mantle AFC curves after Stern and Kilian (1996) (curve 1) and Rapp et al. (1999) (curve 2). Crustal AFC is after Stern and Kilian (1996) (curve 3). The starting point of Curve 1 represents the composition of a pure slab melt which was proposed by Stern and Kilian (1996). The starting point of Curve 2 represents the composition of a metabasaltic or eclogite experimental melt which is not hybridized by peridotite (Rapp et al., 1999). Data for metabasaltic and eclogitic experimental melts (1–4.0 GPa) and mafic–ultramafic intrusive rocks are from sources as in Fig. 3. Field of metabasaltic and eclogite experimental melts hybridized with peridotite is after Rapp et al. (1999). Other fields and symbols are the same as those in Fig. 3.

The AG rocks are characterized by medium to high SiO_2 (59.39–68.94 wt.%) and K_2O contents (2.09–3.86 wt.%) and low $Mg^{\#}$ values (mostly 38–45), which are different from those of typical slab-derived adakites (Martin et al., 2005). Besides inherited cores, zircons from the AG rocks exhibit strongly negative $\varepsilon_{Hf}(t)$ values (−21 to −11). The above geochemical features indicate a significant contribution of old crustal material and preclude an origin through partial melting of subducted oceanic lithosphere or slab-melt-modified peridotitic mantle wedge (Stern and Kilian, 1996; Moyen et al., 2001; Martin et al., 2005). In addition, the very low Cr, Co and Ni contents exclude melt–mantle interaction which commonly occurs when slab-derived melt traverses the mantle peridotite in a wedge above a subducting slab (Martin, 1999; Rapp et al., 1999; Smithies, 2000). The reported low $\varepsilon_{Nd}(t)$ values (−17 to −12) and old Nd model ages (2.5–2.7 Ga) for Neoproterozoic granitoid rocks in the Kuluketage area also support the above conclusions (Zhang et al., 2007). Recent studies reveal that primary mantle-derived adakitic magmas formed by crustal assimilation and fractional crystallization (AFC) processes of parental basaltic magmas show significant systematic variations in geochemistry and isotopic compositions (e.g., MgO, Cr, Ni contents and Sr–Nd–Pb–Hf isotopic values), and usually develop complex compositional zonations in some minerals (e.g., amphibole and clinopyroxene) (Castillo, 2006; Rodriguez et al., 2007; Guo et al., 2009). The low Cr, Co, Ni contents and uniform low $\varepsilon_{Nd}(t)$, $\varepsilon_{Hf}(t)$ values of the AG samples do not support a mantle source and exclude an origin of primary basaltic magmas by AFC processes.

Some studies indicate that adakitic rocks produced by partial melting of delaminated lower crust should exhibit increased MgO, TiO_2 and compatible element abundances because of metasomatism of mantle peridotite (e.g. Cr, Co and Ni) and modified Nd–Hf isotopic systems of the adakitic melts (Kay and Kay, 1993; Chung et al., 2003; Castillo, 2006). Thus, adakitic rocks derived from partial melting of delaminated lower crust are likely to exhibit higher $Mg^{\#}$, $\varepsilon_{Nd}(t)$ and $\varepsilon_{Hf}(t)$ values and lower FeO^T/MgO ratios than primitive melts of lower crust. However, low MgO and TiO_2 contents and compatible element abundances, combined with low $Mg^{\#}$, $\varepsilon_{Nd}(t)$ and $\varepsilon_{Hf}(t)$ values and high FeO^T/MgO ratios, suggest that the AG rocks are unlikely to have been derived from partial melting of delaminated lower crust. In the $Mg^{\#}$ versus SiO_2 diagram (Fig. 8c), these rocks plot in the field of lower crust-derived adakitic rocks, indicating that partial melting was responsible for their origin.

The oldest basement exposed in the northern Tarim Craton are late Archean to early Paleoproterozoic amphibolite and TTGs (Hu

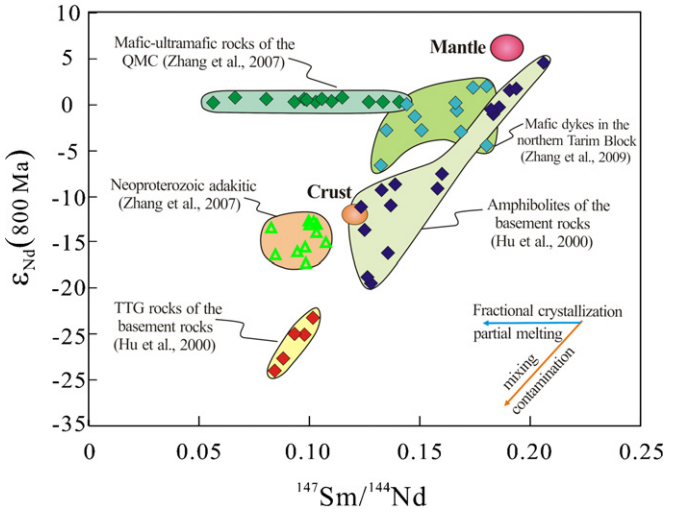

Fig. 9. ε_{Nd} (800 Ma) versus $^{147}Sm/^{144}Nd$ diagrams for the Neoproterozoic granitoids.

et al., 2000; Guo et al., 2003; Long et al., 2010, 2011). Available Sm–Nd isotope and zircon age data show that the amphibolite has $\varepsilon_{Nd}(800)$ values (−20 to −5) higher than those of the AG rocks, whereas the early Paleoproterzoic TTGs have lower $\varepsilon_{Nd}(800)$ values (Fig. 9) (Hu et al., 2000; Hu and Wei, 2006; Guo et al., 2003). Therefore, The AG rocks were probably derived from basement rocks by partial melting of a source consisting of both amphibolite and TTGs. The relatively high Al_2O_3, Sr and very low Y and Yb contents, combined with negligible negative to positive Eu and Sr anomalities, indicate garnet ± plagioclase as residue minerals in the source after melt extraction (Defant and Drummond, 1990; Martin et al., 2005). Low $Mg^{\#}$, $\varepsilon_{Nd}(t)$ and $\varepsilon_{Hf}(t)$ values of the AG rocks reveal an origin from old crustal material, and their low MgO, TiO_2 contents and compatible element abundances indicate no significant addition of mantle material. Therefore, we suggest that the AG rocks formed through partial melting of the basement rocks in the lower part of thickened crust.

5.2. Petrogenesis of the IG

The IG rocks have intermediate SiO_2 contents (58.56–62.06 wt.%) and low ASI indexes (<1), pointing to an I-type granite character (e.g. Chappell and White, 2001). Their low $\varepsilon_{Hf}(t)$ (−12 to −7) values and old zircon Hf two-stage model ages (T^2_{DM} = 2.14–2.46 Ga) suggest a crustal origin. The relatively high Y contents and low Sr contents as well as low Sr/Y and $(La/Yb)_N$ ratios of the IG rocks suggest that no garnet remained as residue in the source after melt extraction. As illustrated by the $(La/Yb)_N$ versus Yb_N diagram (Fig. 8b), the IG samples display an origin through amphibolite melting. Zircons of the IG samples exhibit $\varepsilon_{Hf}(t)$ values slightly higher than those of the AG suite, suggesting that the IG was probably derived from partial melting of a similar source as the AG, but at a shallower depth below the garnet stable field with relevant addition of mantle material, e.g. mixing of mantle-derived magma with the old lower crust.

6. Discussion

6.1. Neoproterozoic thickened crust of the Tarim Craton

The AG suite displays strongly depleted HREE abundances related to LREE and very low Y and Yb contents and thus have high Sr/Y and La/Yb ratios, which are typical geochemical characteristics of adakites (Fig. 8a–b). These characters suggest that garnet was stable in the source as a residual mineral during melt extraction, indicating that the protoliths of the AG underwent amphibolite- to granulite-facies metamorphism in the garnet stability field (Defant and Drummond, 1990; Atherton and Petford, 1993; Rapp and Watson, 1995; Rapp et al., 1999, 2003). Experimental studies have shown that mafic crustal rocks can melt to produce adakitic magmas at pressures equivalent to a crustal thickness of >40–50 km (i.e., 1.2–1.5 GPa) for garnet to be stable within the residual assemblage, such as garnet-amphibolite, amphibole-bearing eclogite and/or eclogite (e.g. Rapp and Watson, 1995; Rapp et al., 1999). Their relatively low Nb/Ta ratios and negative Nb–Ta anomalies indicate that the Neoproterozoic AG rocks were probably generated near the boundary between amphibolite and hornblende-eclogite melting and rutile-eclogite melting (Fig. 8d). The minimum pressure for rutile stability during partial melting of hydrous mafic rocks is at least 1.5 GPa, which equals a depth >50 km (Xiong et al., 2005; Xiong, 2006; Nair and Chacko, 2008). Therefore, a Neoproterozoic thickened crust must have existed in the northern Tarim Craton during the time between 820 and 750 Ma, and its thickness must have been at least 50 km before the AG formed.

6.2. Geodynamic model

The Neoproterozoic mafic–ultramafic–carbonatite complex in the northern Tarim Craton consists of dunite, pyroxenite and carbonatite. These rocks are characterized by pronounced fractionation between LREE and HREE, strong negative Nb–Ta–Ti anomalies and relatively low $\varepsilon_{Nd}(t)$ values varying from +0.5 to +1, and thus were suggested to have been derived from a metasomatized mantle source (Zhang et al., 2007). Similar geochemical features were also found in the Neoproterozoic mafic dykes and mafic volcanic rocks, but with a lower $\varepsilon_{Nd}(t)$ values between −10.8 and +1.8 (Xu et al., 2005; Zhang et al., 2007). In combination with the Neoproterozoic granitoids and felsic volcanic rocks, all these Neoproterozoic igneous rock assemblages were considered to constitute a bimodal suite, formed in a continental rift related to mantle plume activity beneath the Rodinian supercontinent (Xu et al., 2005; Zhang et al., 2006a,b, 2007, 2009b, 2009c).

This study suggests that the Neoproterozoic Kuluketage adakitic rocks with ages between 750 and 820 Ma were derived from partial melting of thickened lower crust (>50 km). Based on the occurrence of ca. 820 Ma metasomatized mantle-derived mafic complexes (Zhang et al., 2007), 760–825 Ma rifting-related mafic dykes (Zhang et al., 2009b, 2009c) and 755 Ma bimodal volcanic rocks (Xu et al., 2005), a tectonic model of underplating of mafic magmas, possibly related to a mantle plume, was proposed to interpret the formation of Neoproterozoic igneous rocks (Fig. 10). During the middle Neoproterozoic, the northern Tarim crust was thickened to over 50 km by underplating of mantle-derived magmas, and metamorphosed into hornblende eclogite to rutile-bearing eclogite. Partial melting of the eclogitic lower crust produced the adakitic rocks by partial melting (820–750 Ma). The mantle magmas metasomatised the lithospheric mantle during ascent and then generated an ultramafic–mafic–carbonatite complex by partial melting. After significant crustal assimilation, the mantle magmas have an obvious decreasing in their $\varepsilon_{Nd}(t)$ values and finally emplaced in a rifting environment, which formed the Neoproterozoic mafic dykes. During this process, the IG suite was generated by partial melting of the shallower crust because of continuous addition of heat provided by the underplated mafic magmas.

6.3. Implications for the Neoproterozoic craton reworking

Based on petrological and geochemical studies of mantle-derived rocks and their xenoliths in the NCC, two representative models (thermo-chemical erosion and delamination) were sug-

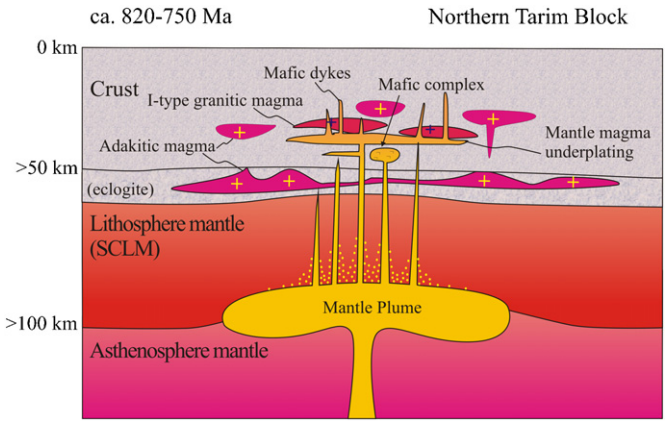

Fig. 10. A proposed model for the generation of Neoproterozoic granitoids in the Kuluketage area through partial melting of thickened lower crust, most likely triggered by underplating of plume-derived magmas.

gested to interpret the reworking of cratonic lithosphere (Griffin et al., 1998; Menzies and Xu, 1998; Xu, 2001; Gao et al., 2002, 2004; Zhang et al., 2003; Xu et al., 2004; Wu et al., 2005, 2008; Zheng et al., 2006; Menzies et al., 2007; Zheng, 2009). Recently, Zhang et al. (2009d) suggested that low-angle subduction of the oceanic crust beneath cratonic lithosphere would have resulted in not only delamination of the ancient subcontinental lithospheric mantle (SCLM) into the asthenosphere, but also transformation of the overlying mantle wedge to the juvenile SCLM. On the basis of geochemical studies of Mesozoic igneous rocks in East China, Chen et al. (2004a) proposed that magmas extracted from the SCLM also provided potential genesis for the lithospheric reworking. Moreover, Lu et al. (1998) and Wilde et al. (2003) suggested that mantle plumes may play an important role in the process of lithospheric reworking, but how a mantle plume reworks a continental lithosphere remains elusive.

In the Kuluketage area, north Tarim Craton, Neoproterozoic mafic and felsic magmatisms and mafic–ultramafic–carbonatite complex were identified and assigned to a bimodal intrusive suite, which was interpreted to have been produced through mantle plume activities beneath the Rodinia supercontinent in a continental rift setting (Xu et al., 2005; Zhang et al., 2006a,b, 2007). Neoproterozoic granitoids (820–750 Ma) in the north Tarim Craton have geochemical characters of adakitic rocks and were derived from partial melting of the thickened lower crust. The adakitic rocks are extensively exposed in the north margin of the Tarim Craton (Xu et al., 2005; Zhang et al., 2007, and this study). Recently, this kind of rocks was also discovered in the central part, although this area is covered with thick sands (Li et al., 2005; Guo et al., 2005). Widespread Neoproterozoic granitoids indicate that the reworking of the lower crust in the north Tarim is related to intensive regional magmatisms. Additionally, the Neoproterozoic mafic complex in this region has positive $\varepsilon_{Nd}(t)$ values (+0.5 to +1, Zhang et al., 2007), indicating that the ancient SCLM was probably metasomatized by underplated materials of mantle plume and became more depleted (Fig. 10). The above lines of evidences suggest underplating of mantle plume-derived magmas had reworked the continental crust of the Tarim Craton and destroyed the stability of its cratonic lithosphere.

Rodinia was a ~1.0 Ga supercontinent and amalgamated by the Grenville-age orogens (Moores, 1991; Dalziel, 1991; Hoffman, 1991). Available paleomagnetic data and paleogeographic reconstructions suggest that the Tarim Craton and South China Block (SCB) have close positions in the Rodinia supercontinent during the Neoproterozoic (Zhao and Cawood, 1999; Chen et al., 2004b; Macouin et al., 2004; Li et al., 2004, 2008; Huang et al., 2005; Xu et al., 2005). The similar paleogeographic positions indicate that the SCB had geological evolution similar to the Tarim Craton and was probably reworked during the Neoproterozoic. Archean basement rocks and overlying Paleo- to Mesoproterozoic sequences are sporadically exposed in the SCB (Qiu et al., 2000; Zhang et al., 2006a,b; Jiao et al., 2009), but extensively distribute in the NCC (Zhao et al., 2001). The difference between the two blocks probably indicates more intensive reworking of lithosphere in the SCB. Although an arc-related tectonic setting was suggested to interpret the Neoproterozoic evolution of the SCB on the basis of geochemistory of adakitic rocks (Zhou et al., 2006; Zhao and Zhou, 2007, 2008), the Neoproterozoic komatiitic basalts, picritic and rifting-related mafic dykes strongly support the existence of Neoproterozoic plume developed underneath the SCB (Wang et al., 2007b; Li et al., 2010). Similarly, the reworking of lithosphere in the SCB can be interpreted by the Neoproterozoic plume and underplating of plume-related mafic magmas, which is supported by the similarities of rock associations and tectonic settings to the Tarim Craton (Li et al., 2002, 2003a,b, 2006). Therefore, mantle plume provides a valid regime in reactivating old cratons. Because of underplating of plume-related magmas, the continental blocks in the Rodinia supercontinent are reworked, which eventually result in the breakup of the supercontinent.

7. Conclusions

(1) The Neoproterozoic adakitic granitoids in the northern Tarim Craton emplaced between 750 and 820 Ma and were originated from partial melting of mixed basement rocks in the lower crust at a depth >50 km.
(2) The normal I-type granitoids formed in the Neoproterozoic (785 Ma) and was generated by partial melting of ancient lower crust at shallower depths than the Neoproterozoic adakitic granitoids.
(3) The crustal thickness in the northern Tarim Craton must have been over 50 km during the Neoproterozoic (750–820 Ma), which was most likely produced by underplating of mantle plume-derived magmas. This model provided an alternative genesis for Neoproterozoic craton reworking not only in Tarim, but also in other cratons in the Rodinia supercontinent.

Acknowledgements

This study was supported by the National Basic Research Program of China (2007CB411308), National Natural Science Foundation of China (40803009, 41073031), Knowledge Innovation Project of CAS (KZCX2-YWQ08-3-6) and CAS/SAFEA International Partnership Program for Creative Research Teams. This is contribution No. IS-1308 from GIGCAS.

Appendix A. Supplementary data

Supplementary data associated with this article can be found, in the online version, at doi:10.1016/j.precamres.2011.02.001.

References

Andersen, T., 2002. Correction of common lead in U–Pb analyses that do not report ^{204}Pb. Chem. Geol. 192, 59–79.
Arndt, N.T., Albarède, F., Lewin, E., 2002. Strange partners: formation and survival of continental crust and lithospheric mantle. J. Geol. Soc. (Lond.) Spec. Publ. 199, 91–103.
Arndt, N.T., Coltice, N., Helmstaedt, H., Gregoire, M., 2009. Origin of Archean subcontinental lithospheric mantle: some petrological constraints. Lithos 109, 61–71.
Atherton, M.P., Petford, N., 1993. Generation of sodium rich magmas from newly underplated basaltic crust. Nature 362, 144–146.
BGMRX (Bureau of Geology and Mineral Resources of Xinjiang Uygur Autonomous Region), 1993. Regional Geology of Xinjiang Uygur Autonomous Region, Peo-

ple's Republic of China, Ministry of Geology and Mineral Resources, Geological Memoirs, Series 1, No. 32. Geological Publishing House, Beijing, pp. 1–400 (in Chinese with English abstract).
Bouvier, A., Vervoort, J.D., Patchett, P.J., 2008. The Lu-Hf and Sm-Nd isotopic composition of CHUR: Constraints from unequilibrated chondrites and implications for the bulk composition of terrestrial planets. Earth Planet. Sci Lett. 273, 48–57.
Boyd, F.R., Gurney, J.J., Richardson, S.H., 1985. Evidence for a 150–200 km thick Archaean lithosphere from diamond inclusion thermobarometry. Nature 315, 387–389.
Boyd, F.R., 1989. Compositional distinction between oceanic and cratonic lithosphere. Earth Planet. Sci. Lett. 96, 15–26.
Carlson, R.W., Irving, A.J., Schulze, D.J., Hearn Jr., B.C., 2004. Timing of precambrian melt depletion and Phanerozoic refertilization events in the lithospheric mantle of the Wyoming Craton and adjacent Central Plains Orogen. Lithos 77, 453–472.
Carlson, R.W., Pearson, D.G., James, D.E., 2005. Physical, chemical, and chronological characteristics of continental mantle. Rev. Geophys. 43, doi:10.1029/2004RG000156.
Castillo, P.R., 2006. An overview of adakite petrogenesis. Chin. Sci. Bull. 51, 257–268.
Chappell, B.W., White, A.J.R., 2001. Two contrasting granite types: 25 years later. Aust. J. Earth Sci. 48, 489–499.
Chen, B., Jahn, B.M., Arakawa, Y., Zhai, M.G., 2004a. Petrogenesis of the Mesozoic intrusive complexes from the southern Taihang Orogen, North China Craton: elemental and Sr-Nd-Pb isotopic constraints. Contrib. Mineral. Petrol. 148, 489–501.
Chen, Y., Xu, B., Zhan, S., Li, Y.G., 2004b. First mid-Neoproterozoic paleomagnetic results from the Tarim Basin (NW China) and their geodynamic implications. Precambrian Res. 133, 271–281.
Chu, N.C., Taylor, R.N., Chavagnae, V., Nesbitt, R.W., Boela, R.M., Milton, J.A., German, C.R., Bayon, G., Burton, K., 2002. Hf isotope ratio analysis using multi-collector inductively coupled plasma mass spectrometry: an evaluation of isobaric interferenee corrections. J. Anal. At. Spectrom. 17, 1567–1574.
Chung, S.L., Liu, D.Y., Ji, J.Q., Chu, M.F., Lee, H.Y., Wen, D.J., Lo, C.H., Lee, T.Y., Qian, Q., Zhang, Q., 2003. Adakites from continental collision zones: melting of thickened lower crust beneath southern Tibet. Geology 31, 1021–1024.
Condie, K.C., 2005. TTGs and adakites: are they both slab melts? Lithos 80 (1–4), 33–44.
Dalziel, I.W.D., 1991. Pacific margins of Laurentia and East Antarctica-Australia as a conjugate rift pair: evidence and implications for an Eocambrian supercontinent. Geology 19, 598–601.
de Wit, M.J., et al., 1992. Formation of an Archaean continent. Nature 357, 553–562.
Defant, M.J., Drummond, M.S., 1990. Derivation of some modern arc magmas by melting of young subducted lithosphere. Nature 347, 662–665.
Dong, F.R., Li, S.L., Mao, S.L., 1998. New knowledge on Tograkbulak complexes. Xinjiang Geol. 16 (1), 31–38 (in Chinese with English abstract).
Gao, S., Rudnick, R.L., Carlson, R.W., McDonough, W.F., Liu, Y.S., 2002. Re-Os evidence for replacement of ancient mantle lithosphere beneath the North China Craton. Earth Planet Sci Lett. 198, 307–322.
Gao, S., Rudnick, R.L., Yuan, H.-L., Liu, X.-M., Liu, Y.-S., Xu, W.-L., Ling, W.-L., Ayers, J., Wang, X.-C., Wang, Q.-H., 2004. Recycling lower continental crust in the North China craton. Nature 432, 892–897.
Gao, S., Zhang, J.F., Xu, W.L., Liu, Y.S., 2009. Delamination and destruction of the North China Craton. Chin. Sci. Bull. 54, 3367–3378.
Gao, Z.J., Chen, J.L., Lu, S.N., Peng, C.W., Qin, Z.Y., 1993. The Precambrian metamorphic rocks. Precambrian Geol. (6) (in Chinese with English abstract).
Griffin, W.L., Zhang, A., O'Reilly, S.Y., Ryan, C.G., 1998. Phanerozoic evolution of the lithosphere beneath the Sino-Korean craton. In: Flower, M., Chung, S.L., Lo, C.H., Lee, Y.Y. (Eds.), Mantle Dynamics and Plate Interactions in East Asia American Geophysical Union Geodynamics Series, vol. 27, pp. 107–126.
Griffin, W.L., Wang, X., Jackson, S.E., Pearson, N.J., O'Reilly, S.Y., Xu, X., Zhou, X., 2002. Zircon chemistry and magma mixing, SE China: in-situ analysis of Hf isotopes. Tonglu and Pingtan igneous complexes. Lithos 61, 237–269.
Griffin, W.L., et al., 2003. The origin and evolution of Archean lithospheric mantle. Precambrian Res. 127, 19–41.
Grifin, W.L., Belousova, E.A., Shee, S.R., Pearson, N.J., O'Reily, S.Y., 2004. Archean crustal evolution in the northern Yilgarn Craton: U-Pb and Hf-isotope evidence from detrital zircons. Precambrian Res. 13l, 23l–282.
Guo, F., Nakamura, E., Fan, W., Kobayashi, K., Li, C., Gao, X., 2009. Mineralogical and geochemical constraints on magmatic evolution of Paleocene adakitic andesites from the Yanji area, NE China. Lithos 112, 321–341.
Guo, Z.J., Zhang, Z.C., Liu, S.W., Li, H.M., 2003. U-Pb geochronological evidence for the early Precambrian complex of the Tarim Craton, NW China. Acta Petrol. Sin. 19 (3), 537–542.
Guo, Z.J., Yin, A., Bobinson, A., Jia, C.Z., 2005. Geochronology and geochemistry of deep-drill-core samples from the basement of the central Tarim basin. J. Asian Earth Sci. 25, 45–56.
Hoffman, P.F., 1991. Did the breakout of Laurentia turn Gondwanaland inside out? Science 252, 1409–1412.
Hu, A.Q., Wang, Z.G., Tu, G.Z., 1997. Geological Evolution and Diagenic and Metallogenetic Regularity in Northern Xinjiang. Science Press, Beijing (in Chinese).
Hu, A.Q., Jahn, B.M., Zhang, G.X., Chen, Y.B., Zhang, Q.F., 2000. Crustal evolution and Phanerozoic crustal growth in northern Xinjiang: Nd isotope evidence, 1. Isotopic characterization of basement rocks. Tectonophysics 328, 15–51.
Hu, A.Q., Wei, G.J., 2006. On the Age of the Neo-Archean Qingir Gray Gneisses from the Northern Tarim Basin, Xinjiang, China. Acta Geol. Sin. 80, 126–134.
Huang, B.C., Xu, B., Zhang, C.X., Li, Y.A., Zhu, R.X., 2005. Paleomagnetism of the Baiyisi volcanic rocks (ca. 740 Ma) of Tarim Northwest China: a continental fragment of neoproterozoic Western Australia? Precambrian Res. 142, 83–92.
Iizuka, T., Hirata, T., 2005. Improvements of precision and accuracy in in situ Hf isotope microanalysis of zircon using the laser ablation-MC-ICPMS technique. Chem. Geol. 220, 121–137.
Jackson, S.E., Pearson, N.J., Griffin, W.L., Belousova, E.A., 2004. The application of laser ablation-inductively coupled plasma-mass spectrometry (LA-ICP–MS) to in situ U-Pb zircon geochronology. Chem. Geol. 211, 47–69.
Jiao, W.F., Wu, Y.B., Yang, S.H., Peng, M., Wang, J., 2009. The oldest basement rock in the Yangtze Craton revealed by zircon U-Pb age and Hf isotope composition. Sci. China Ser. D Earth Sci. 52 (9), 1393–1399.
Kay, R.W., Kay, S.M., 1993. Delamination and delamination magmatism. Tectonophysics 219, 177–189.
King, S.D., 2005. Archean cratons and mantle dynamics. Earth Planet Sci Lett. 234, 1–14.
Lameyre, J., Bowden, P., 1982. Plutonic rock types series—discrimination of various granitoid series and related rocks. J. Volcanol. Geotherm. Res. 14 (1–2), 169–186.
Le Maitre, R.W., 1989. A Classification of Igneous Rocks and Glossary Terms. Recommendations of the International Union of Geological Sciences Subcommission on the Systematics of Igneous Rocks. Blackwell Scientific Publications, Oxford, pp. 1–193.
Li, X.H., 1997. Geochemistry of the Longsheng ophilite from the southern margin of Yangtze Craton, SE China. Geochem. J. 31, 323–337 (in Chinese with English abstract).
Li, X.H., Li, Z.X., Zhou, H., Liu, Y., Kinny, P.D., 2002. U-Pb zircon geochronology, geochemistry and Nd isotopic study of Neoproterozoic bimodal volcanic rocks in the Kangdian Rift of South China: implications for the initial rifting of Rodinia. Precambrian Res. 113, 135–155.
Li, X.H, Li, Z.X., Ge, W.C., Zhou, H.W., Li, W.X., Liu, Y., Wingate, M.T.D., 2003a. Neoproterozoic granitoids in South China: crustal melting above a mantle plume at ca. 825 Ma? Precambrian Res. 122, 45–83.
Li, X.H., Li, Z.X., Wingate, M.T.D., Chung, S.L., Liu, Y., Lin, G.C., Li, W.X., 2006. Geochemistry of the 755 Ma Mundine Well dyke swarm, northwestern Australia: part of a Neoproterozoic mantle superplume beneath Rodinia? Precambrian Res. 146, 1–15.
Li, X.H., Zhu, W.G., Zhong, H., Wang, X.C., He, D.F., Bai, Z.J., Feng, L., 2010. The Tongde Picritic Dikes in the Western Yangtze Block: Evidence for Ca. 800-Ma Mantle Plume Magmatism in South China during the Breakup of Rodinia. J. Geol. 118, 509–522.
Li, Y.J., Song, W.J., Wu, G.Y., Wang, Y.F., Li, Y.P., Zheng, D.M., 2005. Jinning granodiorite and diorite deeply concealed in the central Tarim Basin. Sci. China Ser. D: Earth Sci. 48, 2061–2068.
Li, Z.X., Li, X.H., Kinny, P.D., Wang, J., 1999. The breakup of Rodinia: did it start with a mantle plume beneath South China? Earth Planet. Sci. Lett. 173, 171–181.
Li, Z.X., Li, X.H., Kinny, P.D., Wang, J., Zhang, S., Zhou, H., 2003b. Geochronology of Neoproterozoic syn-rift magmatism in the Yangtze Craton South China and correlations with other continents: evidence for a mantle superplume that broke up Rodinia. Precambrian Res. 122, 85–109.
Li, Z.X., Evans, D.A.D., Zhang, S., 2004. A 90° spin on Rodinia: possible causal links between the Neoproterozoic supercontinent, superplume, true polar wander and low-latitude glaciation. Earth Planet. Sci. Lett. 220, 409–421.
Li, Z.X., Bogdanova, S.V., Collins, A.S., Davidson, A., De Waele, B., Ernst, R.E., Fitzsimons, I.C.W., Fuck, R.A., Gladkochub, D.P., Jacobs, J., Karlstrom, K.E., Lu, S., Natapovm, L.M., Pease, V., Pisarevsky, S.A., Thrane, K., Vernikovsky, V., 2008. Assembly, configuration, and break-up history of Rodinia: A synthesis. Precambrian Res. 160, 179–210.
Long, X.P., Yuan, C., Sun, M., Zhao, G.C., Xiao, W.J., Wang, Y.J., Yang, Y.H., Hu, A.Q., 2010. Archean crustal evolution of the northern Tarim Craton, NW China: Zircon U-Pb and Hf isotopic constraints. Precambrian Res. 180, 272–284.
Long, X.P., Yuan, C., Sun, M., Xiao, W.J., Zhao, G.C., Zhou, K.F., Wang, Y.J., Hu, A.Q., 2011. The discovery of the oldest rocks in the Kuluketage area and its geological implications. Sci. China Earth Sci., doi:10.1007/s11430-010-4156-z.
Lu, F.X., Wang, Y., Chen, M.H., Zheng, J.P., 1998. Geochemical characteristics and emplacement ages of the Mengyin kimberlites, Shandong Province, China. Int. Geol. Rev. 40, 998–1006.
Lu, S.N., 1992. The proterozoic tectonic evolution of Quruqtagh, Xinjiang. J. Tianjin Geol. Miner. Resour. 26–27, 279–292 (in Chinese).
Lu, S.N., Li, H.K., Chen, Z.H., 2003. Characteristic, sequence and ages of Neoproterozoic thermo-tectonic events between Tarim and Yangzi blocks: a hypothesis of Yangzi-Tarim connection. Earth Sci. Front. 10, 321–326 (in Chinese).
Lu, S.N., Li, H.K., Zhang, C.L., Niu, G.H., 2008. Geological and geochronological evidence for the Precambrian evolution of the Tarim Craton and surrounding continental fragments. Precambrian Res. 160, 94–107.
Ludwig, K.R., 2003. User's Manual for Isoplot 3.00. A Geochronological Toolkit for Microsoft Excel. Berkeley Geochronology Center, Special Publication No. 4a, Berkeley, CA.
Macouin, M., Besse, J., Ader, M., Gilder, S., Yang, Z., Sun, Z., Agrinier, P., 2004. Combined paleomagnetic and isotopic data from the Doushantuo carbonates South China: implications for the "snowball Earth" hypothesis. Earth Planet. Sci. Lett. 224, 387–398.
Maniar, P.D., Piccoli, P.M., 1989. Tectonic discrimination of granitoids. Geol. Soc. Am. Bull. 101, 635–643.
Martin, H., 1999. The adakitic magmas: modern analogues of Archaean granitoids. Lithos 46, 411–429.

Martin, H., Smithies, R.H., Rapp, R., Moyen, J.F., Champion, D., 2005. An overview of adakite, tonalite-trondhjemite-granodiorite (TTG), and sanukitoid: relationships and some implications for crustal evolution. Lithos 79, 1–24.

Menzies, M.A., Xu, Y.G., 1998. Geodynamics of the North China craton. Mantle dynamics and plate interaction in east Asia. In: Flower, M., Chung, S.L., Lo, C.H., Lee, Y.Y. (Eds.), Mantle Dynamics and Plate Interactions in East Asia. American Geodynamics, vol. 27. American Geophysical Union, Washington, DC, pp. 155–164.

Menzies, M., Xu, Y.G., Zhang, H.F., Fan, W.M., 2007. Integration of geology, geophysics and geochemistry: a key to understanding the North China Craton. Lithos 96, 1–21.

Moores, E.M., 1991. Southwest U.S.–East Antarctic (SWEAT) connection: a hypothesis. Geology 19, 425–428.

Moyen, J.F., Martin, H., Jayananda, M., 2001. Multi-element geochemical modelling of crust–mantle interactions during late-Archaean crustal growth: the Closepet granite (South India). Precambrian Res. 112, 87–105.

Muir, R.J., Weaver, S.D., Bradshaw, J.D., Eby, G.N., Evans, J.A., 1995. Geochemistry of the Creaceous separation point batholith, New Zealand: granitoid magmas formed by melting of mafic lithosphere. J. Geol. Soc. Lond. 152, 689–701.

Nair, R., Chacko, T., 2008. Role of oceanic plateaus in the initiation of subduction and origin of continental crust. Geology 36, 583–586.

O'Connor, J.T., 1965. A classification for quartz-rich igneous rock based on feldspar ratios. U. S. Geol. Surv. Prof. Pap. 525B, B79–B84.

Pearson, D.G., Carlson, R.W., Shirey, S.B., Boyd, F.R., Nixon, P.H., 1995. Re-Os Sm-Nd, and Rb-Sr isotopic evidence for thick Archaean lithospheric mantle beneath the Siberian craton modified by multistage metasomatism. Geochim. Cosmochim. Acta 59, 959–977.

Petford, N., Atherton, M., 1996. Na-rich partial melts from newly underplated basaltic crust: the Cordillera Blanca Batholith, Peru. J. Petrol. 37, 1491–1521.

Pollack, H.N., 1986. Cratonization and thermal evolution of the mantle. Earth Planet. Sci. Lett. 80, 175–182.

Qiu, Y.M., Gao, S., McNaughton, N.J., Groves, D.I., Ling, W.L., 2000. First evidence of >3.2 Ga continental crust in the Yangtze craton of south China and its implications for Archean crustal evolution and Phanerozoic tectonics. Geology 28, 11–14.

Rapp, R.P., Watson, E.B., 1995. Dehydration melting of metabasalt at 8-32 kbar: implications for continental growth and crust–mantle recycling. J. Petrol. 36, 891–931.

Rapp, R.P., Shimizu, N., Norman, M.D., Applegate, G.S., 1999. Reaction between slab-derived melts and peridotite in the mantle wedge: experimental constraints at 3.8 GPa. Chem. Geol. 160, 335–356.

Rapp, R.P., Shimizu, N., Norman, M.D., 2003. Growth of early continental crust by partial melting of eclogite. Nature 425, 605–609.

Rodriguez, C., Selles, D., Dungan, M., Langmuir, C., Leeman, W., 2007. Adakitic dacites formed by intracrustal crystal fractionation of water-rich parent magmas at Nevado de Longav volcano (36.2 degrees S; Andean Southern Volcanic Zone, central Chile). J. Petrol. 48, 2033–2061.

Shu, L.S., Deng, X.L., Zhu, W.B., Ma, D.S., Xiao, W.J., 2010. Precambrian tectonic evolution of the Tarim Block, NW China: new geochronological insights from the Quruqtagh domain. J. Asian Earth Sci., doi:10.1016/j.jseaes.2010.08.018.

Sleep, N.H., 2003. Survival of Archean cratonal lithosphere. J. Geophys. Res. 108, doi:10.1029/2001JB000169.

Sleep, N.H., 2005. Evolution of the continental lithosphere. Annu. Rev. Earth Planet Sci. 33, 369–393.

Smithies, R.H., 2000. The Archaean tonalite–trondhjemite–granodiorite (TTG) series is not an analogue of Cenozoic adakite. Earth Planet. Sci. Lett. 182, 115–125.

Soderlund, U., Patchett, P.J., Vervoort, J.D., Isachsen, C.E., 2004. The 176Lu decay constant determined by Lu-Hf and U-Pb isotope systematics of Precambrian mafic intrusions. Earth Planet. Sci. Lett. 219, 311–324.

Stern, C.R., Kilian, R., 1996. Role of the subducted slab, mantle wedge and continental crust in the generation of adakites from the Austral Volcanic Zone. Contrib. Mineral. Petrol. 123, 263–281.

Streckeisen, A., 1976. To each plutonic rock its proper name. Earth-Sci. Rev. 12, 1–33.

Sun, S.-S., McDonough, W.F., 1989. Chemical and isotopic systematics of oceanic basalts: implications for mantle composition and processes. vol. 42 In: Saunders, A.D., Norry, M.J. (Eds.), Magmatism in the Ocean Basins Geol. Soc. Spec. Publ, pp. 313–345.

Wang, Q., McDermott, F., Xu, J.F., Bellon, H., Zhu, Y.T., 2005. Cenozoic K-rich adakitic volcanic rocks in the Hohxil area, northern Tibet: lower-crustal melting in an intracontinental setting. Geology 33, 464–468.

Wang, Q., Xu, J.F., Jian, P., Bao, Z.W., Zhao, Z.H., Li, C.F., Xiong, X.L., Ma, J.L., 2006. Petrogenesis of adakitic porphyries in an extensional tectonic setting, Dexing, South China: implications for the genesis of porphyry copper mineralization. J. Petrol. 47, 119–144.

Wang, Q., Wyman, D.A., Xu, J.F., Jian, P., Zhao, Z.H., Li, C.F., Xu, W., Ma, J.L., He, B., 2007a. Early Cretaceous adakitic granites in the Northern Dabie Complex, central China: Implications for partial melting and delamination of thickened lower crust. Geochim. Cosmochim. Acta 71, 2609–2636.

Wang, X.C., Li, X.H., Li, W.X., Li, Z.X., 2007b. Ca 825 Ma komatiitic basalts in South China: First evidence for > 1500 °C mantle melts by a Rodinian mantle plume. Geology 35, 1103–1106.

Wells, M.L., Hoisch, T.D., 2008. The role of mantle delamination in widespread Late Cretaceous extension and magmatism in the Cordilleran orogen, western United States. Geol. Soc. Am. Bull. 120, 515–530.

Wiedenbeck, M., Alle, P., Corfu, F., Griffin, W.L., Meier, M., Oberli, F., Vonquadt, A., Roddick, J.C., Speigel, W., 1995. Three natural zircon standards for U-Th-Pb, Lu-Hf, trace-element and REE analyses. Geostand. Newslett. 19, 1–23.

Wilde, S.A., Zhou, X.H., Nemchin, A.A., Sun, M., 2003. Mesozoic crust–mantle interaction beneath the North China Craton: a consequence of the dispersal of Gondwanaland and accretion of Asia. Geology 31, 817–820.

Woodhead, J., Hergt, J., Shelley, M., Eggins, S., Kemp, R., 2004. Zircon Hf-isotope analysis with an excimer laser, depth profiling, ablation of complex geometries, and concomitant age estimation. Chem. Geol. 209, 121–135.

Wu, F.Y., Lin, J.Q., Wilde, S.A., Zhang, X.O., Yang, J.H., 2005. Nature and significance of the Early Cretaceous giant igneous event in eastern China. Earth Planet Sci Lett. 233, 103–119.

Wu, F.Y., Yang, Y.H., Xie, L.W., Yang, J.H., Xu, P., 2006. Hf isotopic compositions of the standard zircons and baddeleyites used in U–Pb geochronology. Chem. Geol. 234, 105–126.

Wu, F.Y., Xu, Y.G., Gao, S., Zheng, J.P., 2008. Lithospheric thinning and destruction of the North China Craton. Acta Petrol. Sin. 24, 1145–1174.

Wyman, D.A., Kerrich, R., Polat, A., 2002. Assembly of Archean cratonic mantle lithosphere and crust: plume–arc interaction in the Abitibi–Wawa subduction–accretion complex. Precambrian Res. 115, 37–62.

Xie, L.W., Zhang, Y.B., Zhang, H.H., Sun, J.F., Wu, F.Y., 2008. In situ simultaneous determination of trace elements, U-Pb and Lu-Hf isotopes in zircon and baddeleyite. Chin. Sci. Bull. 53, 1565–1573.

Xiong, X.L., Adam, J., Green, T.H., 2005. Rutile stability and rutile/melt HFSE partitioning during partial melting of hydrous basalt: implications for TTG genesis. Chem. Geol. 218, 339–359.

Xiong, X.L., 2006. Trace element evidence for growth of early continental crust by melting of rutile-bearing hydrous eclogite. Geology 34, 945–948.

Xu, B., Jian, P., Zheng, H.F., Zhou, H.B., Zhang, L.F., Liu, D.Y., 2005. U-Pb zircon geochronology and geochemistry of Neoproterozoic volcanic rocks in the Tarim Block of northwest China: implications for the breakup of Rodinia supercontinent and Neoproterozoic glaciations. Precambrian Res. 136, 107–123.

Xu, J.F., Shinjio, R., Defant, M.J., Wang, Q., Rapp, R.P., 2002. Origin of Mesozoic adakitic intrusive rocks in the Ningzhen area of east China: partial melting of delaminated lower continental crust? Geology 12, 1111–1114.

Xu, Y.G., 2001. Thermo-tectonic destruction of the Archaean lithospheric keel beneath the Sino-Korean craton in China: evidence, timing and mechanism. Phys. Chem. Earth (A) 26, 747–757.

Xu, Y.G., Huang, X.L., Ma, J.L., Wang, Y.B., Iizuka, Y., Xu, J.F., Wang, Q., Wu, X.Y., 2004. Crust-mantle interaction during the tectono-thermal reactivation of the North China craton: constraints from SHRIMP zircon U–Pb chronology and geochemistry of Mesozoic plutons from western Shandong. Contrib. Mineral. Petrol. 147, 750–767.

Xu, Y.G., Li, H.Y., Pan, C.J., He, B., 2009. On the timing and duration of the destruction of the North China Craton. Chin. Sci. Bull. 54, 3379–3396.

Zhang, S.B., Zheng, Y.F., Wu, Y.B., Zhao, Z.F., Gao, S., Wu, F.Y., 2006a. Zircon U–Pb age and Hf isotope evidence for 3.8 Ga crustal remnant and episodic reworking of Archean crust in South China. Earth Planet. Sci. Lett. 252, 56–71.

Zhang, S.B., Zheng, Y.F., Zhao, Z.F., Wu, Y.B., Yuan, H., Wu, L.F.Y., 2009a. Origin of TTG-like rocks from anatexis of ancient lower crust: Geochemical evidence from Neoproterozoic granitoids in South China. Lithos 113, 347–368.

Zhang, C.L., Li, Z.X., Li, X.H., Wang, A.G., Guo, K.Y., 2006b. Neoproterozoic bimodal intrusive complex in southwestern Tarim block of NW China: age, geochemistry and Nd isotope and implications for the rifting of Rodinia. Int. Geol. Rev. 48, 112–128.

Zhang, C.L., Li, X.H., Li, Z.X., Lu, S.N., Ye, H.M., Li, H.M., 2007. Neoproterozoic ultramafic-mafic-carbonatite complex and granitoids in Quruqtagh of northeastern Tarim Block, western China: Geochronology, geochemistry and tectonic implications. Precambrian Res. 152, 149–169.

Zhang, C.L., Li, Z.X., Li, X.H., Ye, H.M., 2009b. Neoproterozoic mafic dyke swarms at the northern margin of the Tarim Block, NW China: Age, geochemistry, petrogenesis and tectonic implications. J. Asian Earth Sci. 35, 167–179.

Zhang, H.F, Sun, M., Zhou, X.H., Zhou, M.F., Fan, W.M., Zheng, J.P., 2003. Secular evolution of the lithosphere beneath the eastern North China Craton: evidence from Mesozoic basalts and high-Mg andesites. Geochim. Cosmochim. Acta 67, 4373–4387.

Zhang, Z.Y., Zhu, W.B., Shu, L.S., Su, J.B., Zheng, B.H., 2009c. Neoproterozoic ages of the Kuluketage diabase dyke swarm in Tarim, NW China, and its relationship to the breakup of Rodinia. Geol. Mag. 146, 150–154.

Zhang, J.J., Zheng, Y.F., Zhao, Z.F., 2009d. Geochemical evidence for interaction between oceanic crust and lithospheric mantle in the origin of Cenozoic continental basalts in east-central China. Lithos 110, 305–326.

Zhao, G.C., Wilde, S.A., Cawood, P.A., Lu, L.Z., 1998. Thermal evolution of the Archaean basement rocks from the eastern part of the North China Craton and its bearing on tectonic setting. Int. Geol. Rev. 40, 706–721.

Zhao, G.C., Cawood, P.A., 1999. Tectonothermal evolution of the Mayuan Assemblage in the Cathaysia Block; implications for Neoproterozoic collision-related assembly of the South China Craton. Am. J. Sci. 299, 309–339.

Zhao, G.C., Wilde, S.A., Cawood, P.A., Lu, L.Z., 1999. Thermal evolution of two types of mafic granulites from the North China craton: implications for both mantle plume and collisional tectonics. Geol. Mag. 136, 223–240.

Zhao, G.C., Wilde, S.A., Cawood, P.A., Sun, M., 2001. Archean blocks and their boundaries in the North China Craton: lithological, geochemical, structural and P-T path constraints and tectonic evolution. Precambrian Res. 107, 45–73.

Zhao, J.H., Zhou, M.F., 2007. Neoproterozoic adakitic plutons and arc magmatism along the western margin of the Yangtze Block, South China. J. Geol. 115, 675–689.

Zhao, J.H., Zhou, M.F., 2008. Neoproterozoic adakitic plutons in the northern margin of the Yangtze Block, China: Partial melting of a thickened lower crust and implications for secular crustal evolution. Lithos 104, 231–248.

Zheng, J.P., 2009. Comparison of mantle-derived matierals from different spatiotemporal settings: Implications for destructive and accretional processes of the North China Craton. Chin. Sci. Bull. 54, 3397–3416.

Zheng, J.P., Griffin, W.L., O'Reilly, S.Y., Yang, J.S., Li, T.F., Zhang, M., Zhang, R.Y., Liu, J.G., 2006. Mineral chemistry of peridotites from Paleozoic, Mesozoic and Cenozoic lithosphere: constraints on mantle evolution beneath Eastern China. J. Petrol. 47, 2233–2256.

Zheng, Y.F., Wu, F.Y., 2009. Growth and reworking of cratonic lithosphere. Chin. Sci. Bull. 54, 3347–3353.

Zhou, M.F., Yan, D.P., Wang, C.L., Qi, L., Kennedy, A., 2006. Subduction-related origin of the 750 Ma Xuelongbao adakitic complex (Sichuan Province China): implications for the tectonic setting of the giant Neoproterozoic magmatic event in South China. Earth Planet. Sci. Lett. 248, 286–300.

Zhu, R.X., Zheng, T.Y., 2009. Destruction geodynamics of the North China Craton and its Paleoproterozoic plate tectonics. Chin. Sci. Bull. 54, 3354–3366.